UNIVERSITY OF CALIFORNIA, SAN DIEGO

EFFECTS OF HYALURONIC ACID CONCENTRATION POLARIZATION ON HYDRAULIC PERMEABILITY

A thesis submitted in partial satisfaction of the

requirements for the degree Master of Science

in

Bioengineering

by

Anna Luan

Committee in charge:

Professor Robert L. Sah, Chair
Professor Pedro J. Cabrales
Professor David A. Gough

2012

The Thesis of Anna Luan is approved, and it is acceptable in quality and form for publication on microfilm and electronically:

_____

_____

_____

Chair

University of California, San Diego

2012

TABLE OF CONTENTS

LIST OF FIGURES AND TABLES

ACKNOWLEDGMENTS

I would like to thank my research advisor, Dr. Robert Sah, for his direction and support, and for the opportunity to learn from this community of bright, talented researchers. The training and knowledge I have received in technical skills, scientific communication, and the research process are invaluable.

I would also like to thank my lab mentor, William McCarty, for his continuous guidance and aid. Thank you for your critical eye, careful thought, and ready advice. I am truly fortunate to have had the opportunity to work with you and be the recipient of your mentorship for the past three years. This work would not have been possible without you.

Thank you also to the other members of the CTE lab; and especially Alex Hui, Felix Hsu, Murray Grissom, Jerome Hollenstein, and Johnny Du, who have all shared their knowledge, working space, and humor with me at some point along the way.

Finally, I would like to thank my family: Linda, Harry, and Jeff, for their unwavering support and encouragement. Thank you for keeping me grounded and focused.

ABSTRACT OF THE THESIS

Effects of Hyaluronic Acid
Concentration Polarization
On Hydraulic Permeability

by

Anna Luan

Master of Science in Bioengineering
University of California, San Diego, 2012
Professor Robert L. Sah, Chair

In normal joints, tissues such as synovium and articular cartilage provide resistance to outflow of water and macromolecules in synovial fluid (SF). Hyaluronan (HA) normally contributes to hydraulic outflow resistance under increased pressure by a reduction of the driving force via a concentration polarized layer at the surfaces of the joint capsule [11, 44, 58, 66]. Changes in the synovial joint that occur in osteoarthritis

(OA) and injury, including decreased HA content and joint tissue degeneration, are likely to alter the formation of this layer.

An ultrafiltration model was solved to evaluate the dynamics and steady-state properties of HA concentration polarization across the synovium in health and disease, and the model results were compared to experimental data. Validation simulations were similar to measured transient and steady-state values for concentration and retention. The model predicted that HA at a normal concentration and molecular weight is mostly retained, resulting in physiologically observed intra-articular pressures. Predicted HA retention, concentration distributions, and dynamic hydraulic permeability were altered with decreased initial HA concentration and molecular weight, as observed in disease. In diseased joints, after a period of temporary slight concentration polarization, HA is predicted to be depleted from the joint cavity due to increased loss through the membrane.

These studies provide a foundation for further understanding of hyaluronic acid concentration polarization in the normal and diseased synovial joint by modeling flow of HA solutions through a membrane, as well as the effect of HA concentration and retention on the formation of the concentration polarization layer.

CHAPTER 1

INTRODUCTION

1.1 General Introduction to the Thesis

Previous studies [10, 36, 44, 45, 59] have investigated the relationship between hyaluronan (HA) and permeability, including HA concentration polarization and HA reflection due to molecular sieving by extracellular matrix proteins. The outflow buffering capabilities of hyaluronan (HA) have been well characterized by previous studies: when HA is present, an increase in resistance to trans-synovial fluid filtration from the joint cavity is proportional to the increase in intra-articular pressure [44, 45]. It has been further suggested that this outflow buffering is due to the formation of a highly concentrated HA layer against the synovium, which opposes fluid outflow by creating a concentration polarized layer and raising the osmotic pressure (of HA) at the inner joint interface [10].

It is hypothesized that changes in the synovial joint that take place in osteoarthritis, including changes to both SF content and synovial joint structure, alter hydraulic conductance and the concentration polarization of HA. Such changes in normal flux may further alter SF composition and function within the joint space.

The overall motivation of this thesis work was to contribute to understanding of the concentration polarization of hyaluronic acid and the effects of initial polymer mass, reflection coefficient, and solvent flow rate. Specifically, the aims of this study were to

(1) expand and solve a mathematical model to analyze HA concentration polarization, including steady-state and transient concentration profiles and pressure drops, (2) to assess the validity of the model by comparison with other experimental and theoretical studies, and (3) to apply the model to physiological situations in which HA content and retention are altered.

1.2 Synovial Joint Structure

The synovial joint is a system of interacting components, including articular cartilage, synovium, and synovial fluid (SF). Articular cartilage is a dense, low-friction, wear-resistant tissue that covers the ends of long bones. The synovium, or synovial membrane, is composed of synoviocytes and extracellular matrix. The synovium lines the joint and serves as a pathway between the joint cavity, synovial capillaries, and the underlying subsynovium, which contains lymphatic vessels and synovial capillaries. SF is an ultrafiltrate of blood plasma, and decreases friction against cartilage surfaces by acting as a lubricant during articulation. These components interact to regulate SF composition within the synovial joint **(Figure 1.1)**.

Articular cartilage is a fibrous matrix composed mainly of collagen type II fibrils and chains of glycosaminoglycan (GAG) molecules attached to proteoglycan (PG) core proteins. These elements act together in cartilage to create a high resistance to hydraulic flow [34], which is crucial to its ability to pressurize the interstitial fluid within the joint cavity. Flow through articular cartilage, which has an effective pore size of 2-6.5 nm in radius [40, 48], is normally limited [23, 38, 48], and articular cartilage thus contributes most of the hydraulic resistance of osteochondral tissue in the joint. Adult human articular cartilage occupies a total surface area of approximately 121 cm^2 [16] and is 2-5

mm in thickness [16]. In osteoarthritis, articular cartilage is often present at different levels of degradation across the surface of the joint. At areas of full thickness degradation, whether from osteoarthritis or acute injury, the underlying subchondral bone plate is exposed. The subchondral bone plate is composed of a thin layer of calcified cartilage and 1-2 mm of porous bone. While articular cartilage has a hydraulic permeability of 0.0001-0.002 $mm^2/(MPa \cdot s)$ [39, 41, 43], the subchondral bone plate normally has a hydraulic permeability of approximately 90 $mm^2/(MPa \cdot s)$ [23], and 140-190 $mm^2/(MPa \cdot s)$ in OA [23].

Synovium is a leaky, confining membrane with embedded synoviocytes **(Figure 1.2)**. Synoviocytes of types A ("macrophage-like") and B ("fibroblast-like") are responsible for the secretion of important SF molecules, including HA and other lubricant molecules [22, 64], cytokines [19, 53], HA binding protein [30], and matrix-degrading enzymes [1, 46]. An irregular, complex fibrous network of collagens (types I, III, and V) [3], GAGs [55], PGs [9], and glycoproteins (GPs) occupies the intercellular gaps (1-2 μm). Due to the presence of the ECM, synovium provides resistance to SF outflow [63] with an equivalent pore size between 15-45 nm in radius [35]. In the human knee, synovium occupies a surface area of approximately 277 cm^2 [15] and is approximately 50 μm in thickness [56]. Synovial capillaries, approximately 30 μm from the joint cavity-synovium surface, are fenestrated and heterogeneously permeable. The loose, areolar subsynovium layer beneath the synovium acts as a compliant, low-pressure fluid sink [45]. Lymphatic vessels at the subsynovium-synovium border drain fluid, macromolecules, and particles from the joint cavity.

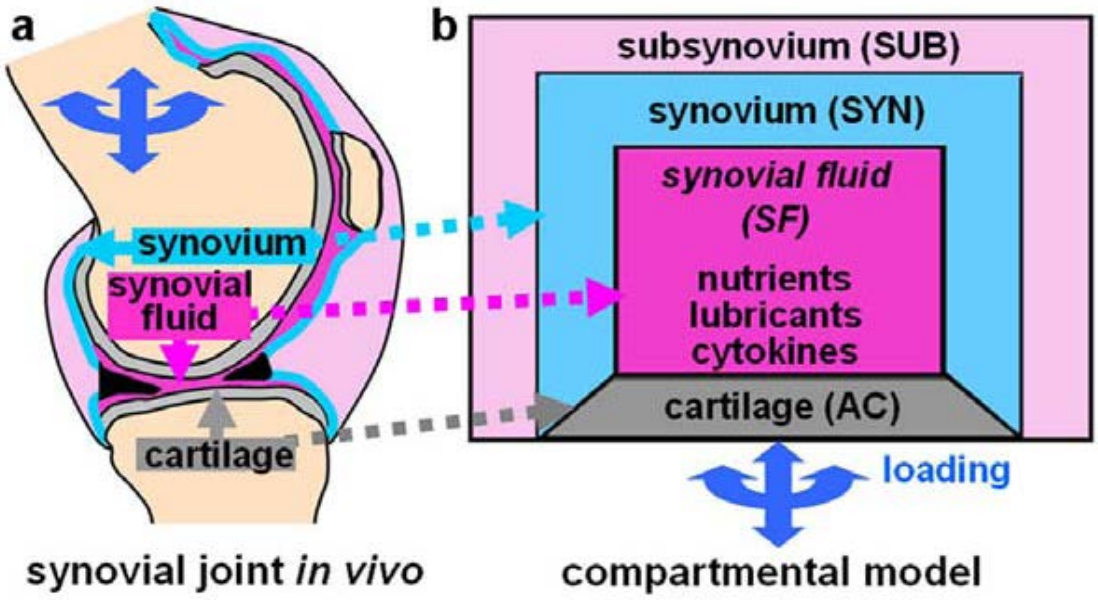

Figure 1.1: Synovial joint components. (**A**) Synovial joints are composed of cartilage, synovium, and SF, (**B**) which are communicating compartments that work together to regulate SF composition. Figure is from [8].

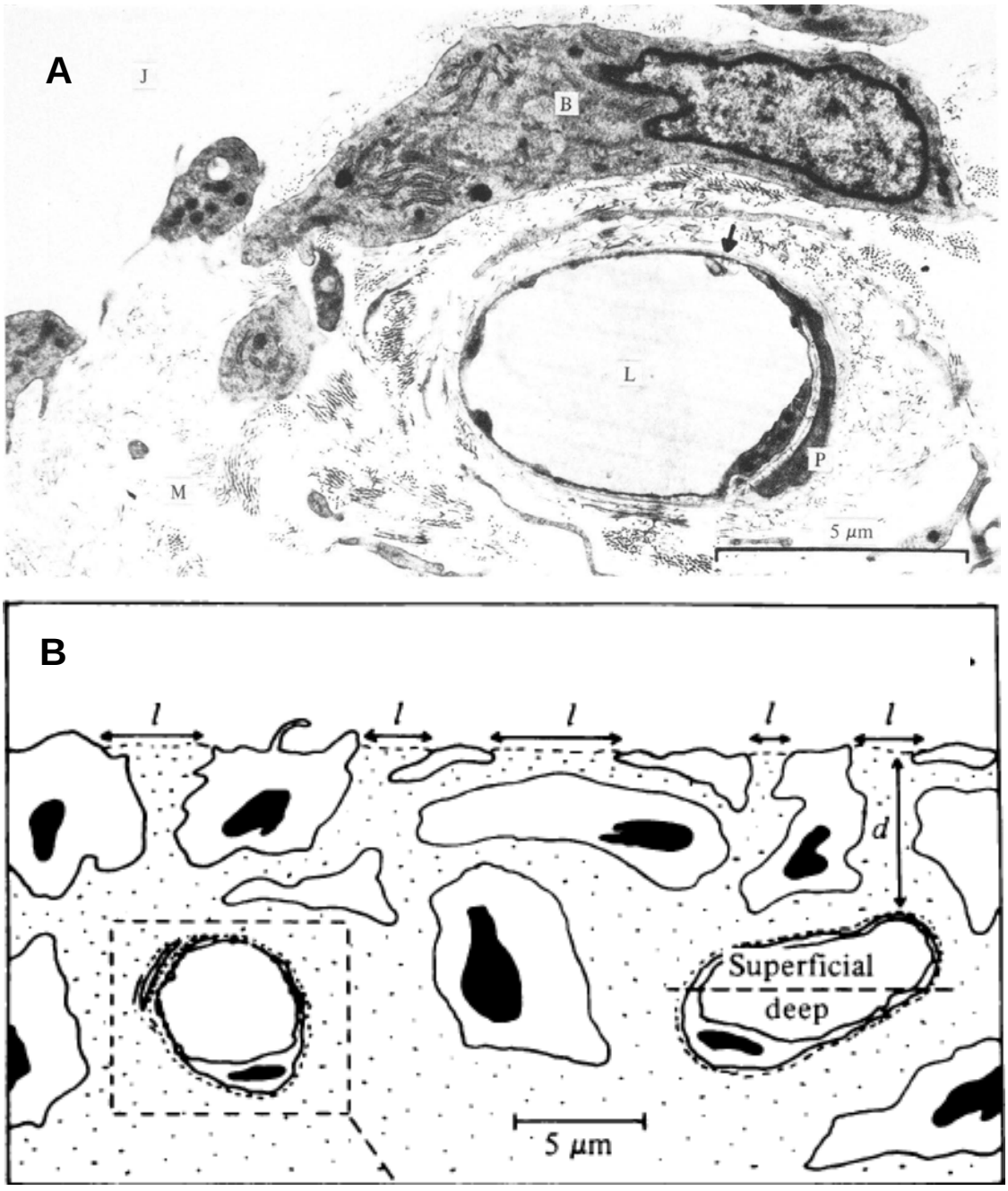

Figure 1.2: Synovium structure. (**A**) Electron micrograph of rabbit knee adipose synovium [32], where J denotes the joint cavity; L, lumen of a fenestrated capillary; P, a pericyte; M, intercellular matrix; and B, a fibroblast-like synoviocyte. (**B**) Schematic of rabbit synovium and two synovial capillaries, where *l* is the length of an intercellular gap and *d* is capillary depth. Modified from [32].

1.3 Synovial Fluid Components

Synovial fluid is a complex mixture of various lubricant molecules, cytokines, plasma proteins, and modulators such as binding molecules and enzymes. Hyaluronic acid (HA) and proteoglycan 4 (PRG4) present in the SF contribute to the boundary lubrication of articular cartilage [52, 65], and are secreted by fibroblast-like synoviocytes within the synovium [22, 26, 47]. A variety of cytokines are secreted by both types of synoviocytes, including IL-1β, TGF-β1, TNF-α, IL-8, and IL-17 [19, 53]. Molecules such as HA binding proteins and cytokine antagonists interact with these components, and enzymes such as hyaluronidase and collagenase allow for degradation and turnover of SF and matrix components. Water, albumins, and globulins enter SF through ultrafiltration from synovial capillaries.

HA is an anionic polysaccharide composed of repeating D-glucuronic acid and N-acetyl-D-glucosamine dimers [20]. Each disaccharide has a length of 0.95 nm, radius of approximately 0.5 nm [17], and molecular weight of 400 Da. Physiologically, the total molecular weight of an HA molecule may range between 10^5 and 10^7 [28]. Normal SF contains HA at concentrations between 1-4 mg ml^{-1}, while HA concentration is lowered in osteoarthritis at 0.7-1.1 mg ml^{-1}, and rheumatoid arthritis at 0.8-1.5 mg ml^{-1} [42].

Influx and efflux of joint fluid is directed by pressure changes within the joint. During extension, the pressure in the joint cavity becomes subatmospheric and net transsynovial flow is directed into the joint cavity [34]. During flexion and loading, pressurization of the intra-articular SF drives fluid out of the joint cavity and into the lymphatic system. The normal synovial knee joint cavity maintains a volume of approximately 1-2 ml of SF [57] and transsynovial flow varies between approximately 10-30 µl min^{-1} [31].

1.4 Concentration Polarization and Outflow Buffering

In aqueous solution, the expanded coil configuration of HA has a radius of gyration (R_g) of between 100-200 nm [20], causing adjacent molecular domains to overlap at HA concentrations at or above approximately 1 mg ml^{-1} [59]. Although HA in solution has domains of 100-200 nm in radius, and synovium has sieving properties equivalent to those of cylindrical pores of 33-59 nm in radius [58], imperfect reflection ($\sigma < 1$) occurs because the HA chain is flexible and can deform to access pores smaller than R_g. Estimates show that the equivalent solid sphere radius of HA is much smaller than R_g [49, 61]. For a 0.2 mg/ml HA solution (average molecular weight 2.1 MDa) infused at a rate of between 10 to 67 µl/min through synovium, the reflection coefficient has been reported to be approximately 0.95 [62], and increased with time due to membrane fouling.

Several previous studies [36, 59, 62] have investigated the molecular sieving of HA by extracellular matrix (ECM) components. Selective filtration of HA through the synovium may be described as analogous to an ultrafiltration system, in which a fraction of the macromolecules are rejected by the membrane and remain upstream. The accumulation of these retained molecules against the membrane surface, and the associated formation of a concentration gradient upstream of the membrane, is a process called concentration polarization. It has been suggested that, in the synovial joint, a highly concentrated HA layer against the synovium opposes fluid outflow [10].

The formation of a concentration polarization layer decreases filtration through osmotic and hydrostatic pressure differences, and an increase in the membrane resistance itself [54]. First, the high concentration at the surface of the membrane induces a large osmotic pressure difference across the membrane [28, 36]. This pressure opposes outflow and can increase the driving pressure required to maintain a constant flow rate. Second, because the solvent must flow through the concentration polarization layer, the structure of the layer itself may contribute to flow resistance [54]. Finally, clogging of the membrane pores by solute molecules can decrease effective pore size and dramatically increase flow resistance.

1.5 Previous Studies in Synovial Fluid Transport and Concentration Polarization

Governing Equations for Concentration Polarized Layers

We can consider the HA concentration polarized layer to be analogous to a porous medium that is affected by osmotic pressure [27, 28]. Incompressible one-dimensional flow through a porous medium is typically described using Darcy's Law [7], which relates the flow rate and pressure gradient for flow in a porous medium:

$$\frac{dP}{dz} = \frac{\mu}{k}\frac{Q}{A} \tag{1}$$

where dP/dz is the hydrostatic pressure gradient (Pa/m), μ is the solvent dynamic viscosity (Pa·s), k is the hydrodynamic layer specific hydraulic conductivity or permeability (m^2), Q is the volumetric solvent flow rate (m^3/s), and A is the cross-sectional area of the flow (m^2).

However, solvent molecules in the concentration polarization layer are subject to forces that can be formulated as chemical potential gradients within the layer and expressed as a local osmotic pressure [21, 27]. Thus, Johnson [27] proposed a modified Darcy's Law in which the net force driving the solvent is the difference between the applied hydrodynamic pressure and the osmotic pressure:

$$\frac{d\left(P'-\Pi(c)\right)}{dz} = \frac{\mu}{k(c)}\frac{Q}{A} \tag{2}$$

where Π is the concentration-dependent osmotic pressure of the solution and k is the concentration-dependent permeability of the layer.

We assume the following general power law equations for the osmotic pressure and permeability of HA solutions [27]:

$$\Pi(c) = bc^n \quad (3)$$

$$k(c) = ac^{-m} \quad (4)$$

where the physicochemical variables *a*, *b*, *m*, and *n* are empirically determined and are dependent on solvent type, ionic strength, pH, temperature, impurities, and polymer MW distribution [21]. **Table 1.1** summarizes estimates of these variables for various HA solutions from published studies.

Osmotic pressure Π of a polymer solution can be expressed in terms of concentration by a virial expansion in which the coefficients are dependent on the polymer MW distribution and solution ionic conditions:

$$\Pi(c) = A_1 c + A_2 c^2 + A_3 c^3 + \ldots \quad (5)$$

and where, according to van't Hoff's law, the first coefficient A_1 is [66]:

$$A_1 = \frac{RT}{M_n} \quad (6)$$

R is the gas constant ($cm^3 \cdot MPa/[mol \cdot K]$), *T* is the temperature (K), and M_n is the number-average molecular weight of the polymer (g/mol). For HA solutions in our range of interest, the coefficient A_1 is small and Equation (5) is dominated by the second order term [21, 27], such that we may use Equation (3) with a value of $n = 2$ as an expression for osmotic pressure.

Steady-State Concentration Profile

Johnson et al. [27, 28] propose that the net force on the polymer molecules is zero within the steady-state polarized layer because the molecules are not accelerating. Thus, at steady-state, the drag force exerted on the polymer molecules by the moving solvent must be balanced by the effective force of the osmotic pressure [27, 28]:

$$\frac{d\Pi}{dz} = -\frac{\mu Q}{k(c)A} \tag{7}$$

By substituting the general power law equations for osmotic pressure and permeability into this force balance, and then integrating from a distance z to the length of the final steady-state concentration polarized layer l_f, an equation describing the steady-state concentration distribution within the layer may be obtained [21]:

$$c(z) = \left[\frac{\mu Q(n-m)(l_f - z)}{abnA}\right]^{1/n-m} \tag{8}$$

Then, by applying conservation of mass, where c_0 is the concentration of HA initially loaded in a layer of thickness l_0,

$$\int_0^{l_f} c(z)dz = c_0 l_0 \tag{9}$$

Gowman and Ethier calculated the final concentration polarization layer thickness for a completely retained polymer solution [21]:

$$l_f = \left[\frac{abnA}{\mu Q(n-m)}\right]^{1/n-m+1}\left[\frac{n-m+1}{n-m}c_0 l_0\right]^{n-m/n-m+1} \tag{10}$$

The concentration at the membrane surface ($z = 0^+$) at steady-state was thus determined by combining these equations [21]:

$$C_{mem} = \left[\frac{\mu Q(n-m+1) C_0 l_0}{abnA} \right]^{1/(n-m+1)} \tag{11}$$

Steady-State Pressure Drop

The hydrostatic pressure drop across the steady-state concentration polarization layer may be calculated using Darcy's Law, which relates the flow rate and pressure gradient for flow in a porous medium:

$$\frac{dP}{dz} = \frac{\mu}{k(c)} \frac{Q}{A} \tag{12}$$

where P is the difference between the applied hydrodynamic and the osmotic pressure in Johnson's modified Darcy's Law [27], and the concentration-dependent hydraulic permeability $k(c)$ is characterized by Equation (4).

The expression can be integrated from the membrane surface to the steady-state layer thickness l_f , substituting in the steady-state concentration distribution equation, to obtain the total pressure drop across the final layer and membrane:

$$\Delta P = \frac{bn}{n-m} \left[\frac{\mu Q(n-m+1)}{abnA} C_0 l_0 \right]^{n/(n-m+1)} \tag{13}$$

By combining the polymer force balance in Equation (7) and modified Darcy's Law in Equation (2), Johnson et al. [28] argue that the pressure gradient within the steady-state layer is zero:

$$\frac{dP'}{dz} = 0 \tag{14}$$

Therefore, they concluded that the pressure drop must be due to the osmotic pressure of the polymer solution across the membrane [27] from the increased HA concentration at the membrane surface such that:

$$\Delta P = \Pi\left(c_{mem}\right) \tag{15}$$

Peppin and Elliot [54] argued that Johnson et al.'s theoretical argument was inexact due to an assumption of negligible intermolecular interactions; however, they concluded that the pressure variations across the layer were insignificant relative to the overall pressure.

Transient Dynamics

The dynamics of concentration polarization of HA remains to be solved analytically or numerically, and applied to physiological conditions of health and disease. A transient model would help to elucidate time-dependent properties of concentration polarization, and would be helpful in understanding in vitro and in vivo perfusion processes. Thus, the overall motivation of this study was to contribute to understanding of the concentration polarization of hyaluronic acid and the effects of initial polymer mass, reflection coefficient, and solvent flow rate. Specifically, the objectives of this study were to (1) expand and solve a mathematical model to analyze HA concentration polarization, including steady-state and transient concentration profiles and pressure drops, (2) to assess the validity of the model by comparison with other experimental and theoretical studies, and (3) to apply the model to physiological situations in which HA composition and retention are altered. The main findings, their significance, and future research directions are discussed in Chapters 2 and 3.

Table 1.1: Physicochemical parameters for osmotic pressure and permeability of various HA solutions calculated in published studies.

Property	Parameter Values	Reference	Comments
Osmotic Pressure $\Pi(C) = bC^n$ (dyn/cm^2)	b = 2.55 x 10^8 (cm^5/g·s^2)	Johnson (1987)	High HA concentration; S > 150 mM
	b = 3.34 x 10^8	Gowman (1996), Peitzsch & Reed (1992)	Up to 10% HA; 10 mM NaCl
Permeability $k(C) = aC^{-m}$ (cm^2)	a = 2.92 x 10^{-16} (g/cm) m = 1.47	Ethier (1986)	0.01%-1.0% HA; 200 mM NaCl
	a = 5.74 x 10^{-16} m = 1.34	Lam & Bert (1990)	0.04%-0.28% HA; 200 mM NaCl
	a = 23.9 x 10^{-16} m = 1.02	Jackson & James (1982)	0.05%-1.5% HA S = 25.4 mM Phosphate buffer

CHAPTER 2

A MODEL OF HYALURONIC ACID CONCENTRATION POLARIZATION: EFFECTS OF MASS, REFLECTION, AND FLOW RATE

2.1 Summary

In normal synovial joints, hyaluronan (HA) is selectively retained in the joint cavity by the synovial lining, leading to the high HA concentration that gives synovial fluid (SF) its lubricating functions. Under increased intra-articular pressure, the formation of an HA concentration polarization layer normally resists fluid outflow due to an osmotic pressure difference across the synovium [11, 44, 58, 66]. It is hypothesized that changes in the synovial joint that occur in osteoarthritis (OA) and injury, including decreased HA concentration, decreased HA MW, and degeneration of joint capsule tissues, are likely to alter the formation of this layer. This study aims to further the understanding of HA concentration polarization in health and disease by modeling the effects of synovial HA composition on the formation of a concentration polarization layer and its fluid-resistance properties. An ultrafiltration model was modified and solved to evaluate the dynamics and steady-state properties of HA molecular sieving and concentration polarization in health and disease, and model

predictions were compared to experimental data. The model predicted that normal HA retention results in physiologically observed intra-articular pressures and contributions to hydraulic resistance. Predicted HA retention, joint space HA concentration distributions, and dynamic hydraulic permeability were altered with parameters characteristic of pathologic SF composition, such as decreased initial HA concentration and molecular weight. The model predicted that in diseased joints, after an initial 2 hours of slight concentration polarization at the membrane surface, HA is depleted from the joint cavity due to steady loss through the membrane. These studies extend current understanding of hyaluronic acid concentration polarization in the synovial joint by modeling flow of HA solutions through a membrane. In addition, this study supports the concentration polarization hypothesis for HA in healthy joint, but suggests that altered molecular sieving may lead to impaired HA and fluid retention under extended flow in disease and injury.

2.2 Introduction

Synovial fluid (SF) is a mixture of various lubricant molecules, cytokines, plasma proteins, and protein modulators. Hyaluronan (HA, or hyaluronic acid) present in the SF decreases friction against cartilage surfaces by contributing to the boundary lubrication of articular cartilage [52, 65], and is secreted by fibroblast-like synoviocytes within the synovium [22, 26, 47]. HA is an anionic polysaccharide composed of repeating D-glucuronic acid and N-acetyl-D-glucosamine dimers [20]. Physiologically, the total molecular weight of an HA molecule may range between 10^5 and 10^7 Da [5, 28], and is present at concentrations of 2-4 mg ml^{-1} in normal SF.

Influx and efflux of joint fluid is directed by pressure changes within the joint. The majority of flow in the normal synovial joint is transsynovial, as flow through articular cartilage is normally limited [23, 38, 48]. During extension, the pressure in the joint cavity becomes subatmospheric and net transsynovial flow is directed into the joint cavity [34]. During flexion and loading, pressurization of the intra-articular SF drives fluid out of the joint cavity and into the areolar subsynovium layer beneath the synovium, which acts as a low-pressure fluid sink [45]. The synovium, or synovial membrane, lines the joint and serves as a pathway between the joint cavity, synovial capillaries, and lymphatic vessels at the subsynovium-synovium border. An irregular, complex fibrous network of collagens [3], GAGs [55], PGs [9], and glycoproteins (GPs) occupies the intercellular gaps; this extracellular matrix (ECM) network provides resistance to transsynovial fluid outflow [59, 63].

The synovium resists fluid efflux and, to a much greater degree, HA outflow [59]. The ECM of the synovial interstitium allows water and small molecules to permeate more readily than macromolecules, leading to selective trapping of high molecular weight (MW) species, including HA, in the joint cavity. Imperfect retention occurs because the HA chain is flexible and can deform to access pores, and estimates show that the equivalent solid sphere radius of HA is much smaller than its radius of gyration R_g [49, 61]. This "molecular sieving" [60, 62] maintains a high concentration of HA in the SF, which is physiologically important for the lubricating function of SF. The retention of HA in the joint cavity may also decrease the need for additional HA production by synoviocytes [12].

The accumulation of these retained molecules against the membrane surface results in a concentration polarization layer, in which a highly concentrated layer of HA develops next to the synovium. It has been suggested that, in the synovial joint, this concentration polarization layer of HA against the synovium opposes fluid outflow ("outflow buffering") [10, 36, 37]. First, the high concentration at the surface of the membrane induces a large osmotic pressure difference across the membrane [28, 36]. This pressure opposes outflow and can increase the driving pressure required to maintain a constant flow rate. Second, because the solvent must flow through the concentration polarization layer, the structure of the layer itself may contribute to flow resistance [54]. Finally, clogging of the membrane pores by solute molecules can decrease effective pore size and dramatically increase flow resistance [21]. These fluid and molecular retention effects may be especially important in periods of maintained flexion of the joint [10].

Arthritis and joint injury may result in significant changes in SF composition and joint tissue structure, which can impact the concentration polarization and outflow buffering effects of HA in the synovial cavity. Diseased joints have dramatically increased SF volume [14, 25, 57] decreased HA concentration [4, 5, 14], and decreased HA MW [4, 5, 14]. Activation of matrix-degrading enzymes in inflamed joints [24, 29] and the degradation of cartilage characteristic of osteoarthritis may lead to changes in the pore characteristics of the joint tissues. Sabaratnam et al. [59] estimated that the equivalent pore radius of synovium increased to 192-336 nm after chymopapain treatment. These changes may individually and cumulatively contribute to decreased fluid and HA retention in the synovial cavity in injury and disease **(Figure 2.1)**.

The selective filtration of HA through synovium may be modeled as an ultrafiltration system, in which an HA solution is perfused through a filter membrane. A fraction of the macromolecules are rejected in front of the membrane, creating a progressive build-up of an HA concentration polarization layer over time [36]. Experimental studies have been reported for pressure-flow relationships, concentration distributions, and overall HA retention fractions. Additionally, several studies have attempted to develop theoretical relationships characterizing the concentration polarization of HA and its effects on pressure [6, 21, 28, 54]. However, a theoretical model of the dynamics of HA molecular sieving and concentration polarization has not yet been applied to physiological conditions of health and disease.

Thus, we hypothesized that a theoretical dynamic model of HA convection, diffusion, and reflection across a semi-permeable membrane could be used to characterize and predict transient and steady-state HA concentration polarization, HA

retention, and hydraulic membrane permeability. The objectives of this study were to (1) expand and solve a mathematical model to analyze HA concentration polarization, including steady-state and transient concentration profiles and pressure drops, (2) to assess the validity of the model by comparison with other experimental and theoretical studies, and (3) to apply the model to physiological situations in which HA composition and retention are altered.

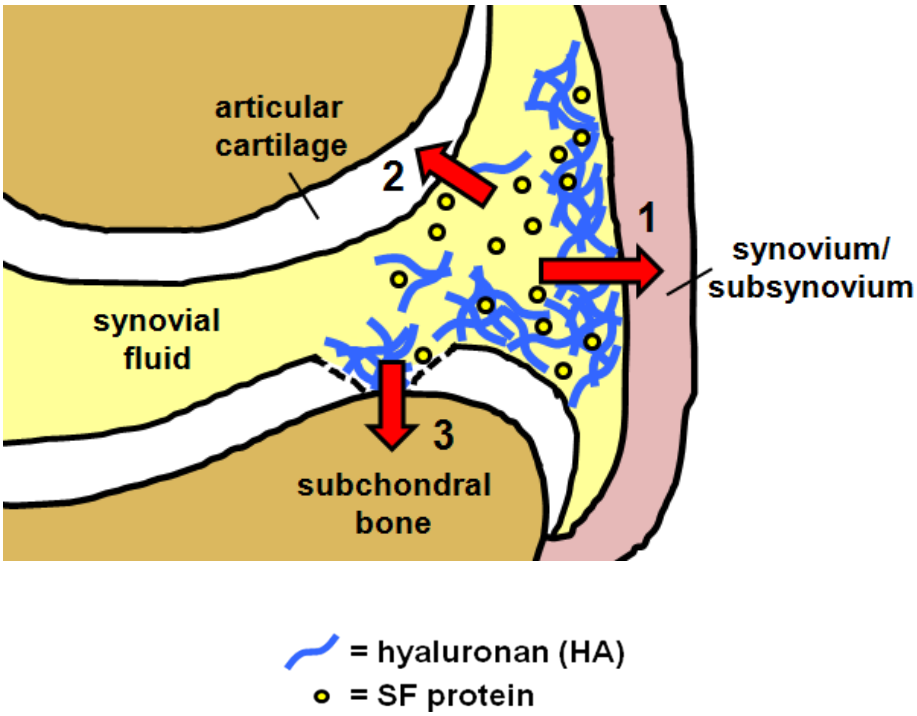

Figure 2.1: Schematic of pathways for SF outflow in the synovial joint. Fluid flow typically occurs through (1) the synovium, and is limited through (2) articular cartilage. However, degradation of the articular cartilage exposes (3) the underlying subchondral bone.

2.3 Model

Convection-Diffusion Model Set-Up

The one-dimensional model of concentration polarization used in the study **(Figure 2.2)** assumes an initial uniform HA concentration for a distance l_0 from the membrane, which we assume reflects HA at a fraction σ(t) at distance z = 0. The HA solution (of initial uniform concentration c_0 and total initial mass m_0) is perfused with pure solvent at filtration velocity U, at a constant volumetric filtration rate Q over a cross-sectional membrane area A over time t, creating a polarized layer of z-dependent concentration c of HA with diffusion coefficient $D(c)$. The HA concentration at the upstream surface of the membrane ($z = 0^+$) is defined as $c_{mem}(t)$. Variables in the model and their units are listed in **Table 2.1**. This model assumes that there are no cross-stream concentration gradients.

The reflection coefficient, σ, is defined as the maximum ability of the membrane to reflect a given solute, and is the fraction of HA retained upstream at the membrane surface such that when no solute passes through the membrane, σ = 1. The reflection coefficient is dependent on filtration rate, HA MW [59], and HA concentration [13, 51].

At any thin slice within the concentration layer, $0^+ < z < l_0$, the concentration is defined by the equilibrium between convective transport toward the membrane and Fick's diffusion away from the membrane:

$$\frac{\partial c}{\partial t} = U\frac{\partial c}{\partial z} + \frac{\partial}{\partial z}\left(D(c)\frac{\partial c}{\partial z} \right) \qquad (1)$$

Initially, the HA is loaded as a layer of length l_0 and concentration c_0 such that the initial condition is:

$$c(z, t=0) = c_0 f(z) \tag{2}$$

$$f(z) = \begin{cases} 1, & 0 \le z < l_0 \\ 0, & z \ge l_0 \end{cases} \tag{3}$$

For *in vitro* experimental ultrafiltration set-ups, where a supply of pure solvent is perfused continuously through the HA solution at moderate flow rates, we assume a boundary condition in which the concentration of HA will remain zero at a distance far upstream of the membrane ($z = L$, where $L >> l_0$):

$$c(L, t) = 0 \tag{4}$$

Also, at the membrane boundary $z = 0^+$, we can apply a boundary condition characterizing a mass balance between diffusion away from, convection towards, and loss through the membrane:

$$-D(c)\left.\frac{\partial c}{\partial z}\right|_{z=0^+} = U\sigma(t)\cdot c(0^+, t) \tag{5}$$

dependent on filtration rate, HA MW [59], and HA concentration [13, 51].

However, in enclosed systems such as the synovial cavity, Equation (4) may not apply. While the experimental ultrafiltration set-up is essentially open-ended to diffusion of HA upstream, the possible HA layer thickness *in vivo* is limited by the dimensions of the joint cavity. In these scenarios, we can instead apply a zero-flux boundary condition at $z = l_0^-$, where l_0 is then defined as the center of the joint space in a symmetry model, and l_0^- is directly next to it:

$$-D(c)\left.\frac{\partial c}{\partial z}\right|_{z=l_0^-} = U \cdot c\left(l_0^-, t\right) \qquad (6)$$

By applying this boundary condition, we specify that diffusive and convective flux balance each other at $z = l_0^-$, such that there is no flux across the center of the joint space $z = l_0$.

Diffusion Coefficient

The HA diffusion coefficient changes as a function of HA concentration. While Brownian motion of HA decreases with concentration due to the formation of an HA network structure [67], the concentration inhomogeneity of HA produces a mutual diffusion coefficient that increases with concentration. Wik and Comper have proposed the following equation [67]:

$$D(c) = (3.93 + 4.26\,c) \times 10^{-8}\ \text{cm}^2\text{s}^{-1} \qquad (7)$$

In this model, fixed HA diffusion coefficients between 0.1-4 x 10^{-6} cm^2s^{-1} are assumed for each simulation **(Table 2.2)**, rather than using a variable diffusion coefficient across the simulation space. This simplification was chosen to avoid oscillations in the solutions where the concentration-dependent diffusion coefficient would be too low.

Reflection Coefficient

While measurements have been made for overall retention of HA solutions perfused through synovium, the reflection coefficient often varies over time [6]. Barry et al. [6] obtained experimental transient HA concentration profiles from integrated laser beam deflections, and calculated reflection coefficients from the observed mass in the

flow cell at certain time intervals. They concluded that the reflection coefficient of HA across the membrane increased with time of perfusion until reaching approximately perfect reflection ($\sigma = 1$) at 20 h [6], however, it is more useful to understand how the reflection coefficient changes with HA concentration. A plot of HA concentration at the membrane surface against observed reflection coefficient, at time intervals reported in the study, exhibits a linear relationship until a critical HA concentration, above which the reflection coefficient is 1 **(Figure 2.3A)**.

Exact mathematical relationships describing the effects of HA concentration, HA molecular weight, membrane pore size, and solvent flow rate on the reflection coefficient are not known. However, using the linear relationship between membrane surface concentration and the reflection coefficient observed in Barry et al., estimates may be made to develop an approximate reflection coefficient as a function of $c_{mem}(t)$ for the model in this study.

A theoretical baseline σ_0 may be estimated using the relative sizes of the membrane pores and the solute. For a pore of radius r_p and a solid, spherical solute of radius r_s, the approximate solute reflection coefficient σ can be related to r_s/r_p through the solute partition coefficient ϕ, which is the complement of the steric exclusion fraction for solute in a narrow pore [2, 13]:

$$\phi = \left(1 - \frac{r_s}{r_p}\right)^2 \tag{8}$$

$$\sigma = (1 - \phi)^2 \tag{9}$$

$$\sigma = \left(1 - \left[1 - \frac{r_s}{r_p}\right]^2\right)^2 \qquad (10)$$

The term $1 - r_s/r_p$ describes the radial space available to the solute relative to water. If $r_s \geq r_p$, $\sigma = 1$. Assuming that the equivalent spherical radius r_s of an HA molecule is directly proportional to its radius of gyration R_g, we can estimate the reflection coefficients σ of various HA solutions through membranes of different pore sizes. Flory [18] and Johnson et al. [28] showed that, for a given solvent and polymer, the radius of gyration of a polyelectrolyte in solution varies with molecular weight as:

$$R_g \sim M^{0.6} \qquad (11)$$

where M is the molecular weight of the HA. Thus, using the MW and reflection data reported by Barry et al., transient reflection coefficients were estimated for each simulation case **(Figure 2.3B)**.

Reflection coefficients as a function of $c_{mem}(t)$ were approximated using the HA MW and membrane pore size in each simulation case **(Figure 2.3B)**. Reflection was estimated to increase with c_{mem} at the rate observed by Barry et al., such that the expression took the general form for $\sigma < 1$:

$$\sigma(t) = 47.341 c_{mem}(t) + \sigma_0 \qquad (12)$$

The variable σ_0 was estimated using Equation (10), where r_s is relative to the MW and effective solute radius calculated for the HA used by Barry et al.:

$$r_s = 5.276\left(\frac{M}{434000}\right)^{0.6} nm \qquad (13)$$

Using this expression, the reflection of HA in the model at time *t* is dependent on MW, membrane pore size, and accumulation of HA at the membrane surface.

Model Parameters

Model predictions were compared to experimental data by using experimental parameters from published studies. Gowman and Ethier [21] loaded an initial 5.2 mg of HA (nominal weight average M_w = 605,000; number average M_n = 434,000) in 1.3 ml of phosphate buffer (ionic strength 28.5 mM) and perfused pure solvent through at a flow rate of 0.131 μm s^{-1} through a 0.015 μm Nuclepore membrane. The flow cell size was such that the initial layer length was 1.02 cm and the linear solvent velocity was 0.131 μm s^{-1}.

Additionally, results from the model were compared with previous experimental perfusion studies (Appendix A). In these studies, 0.75 mg of HA in 750 μl of phosphate buffered saline (PBS) were loaded into a flow cell of area 0.503 cm^2. HA of both low (600-810 kDa) and high (~4 MDa) molecular weight was used. Pure solvent was perfused through the solution at 2 μl min^{-1} until a steady-state pressure was reached. The pressure upstream was measured with a Validyne pressure transducer (DP45, Validyne Engineering), and the pressure downstream was open at atmospheric pressure.

The total surface area of synovium in the human knee joint is approximately 277 cm^2 [15]. Synovium has sieving properties equivalent to cylindrical pores of between 15-45 nm in radius [35]. Joint tissue pore radius is modeled to be between 150-300 nm in disease, to reflect ECM degradation and/or exposure of the subchondral bone plate. Transsynovial volumetric flow varies between approximately 10-30 μl min^{-1} [31]. Normal human knee joint cavities contain approximately 1-2 ml of SF [57], while

between 20-40 ml of SF are often recovered from arthritic joints [14]. The initial HA layer length l_0 was approximated as the volume of SF divided by the surface area of synovium. Concentrations of HA in SF range from approximately 2-4 mg ml^{-1} in normal joints, and 0.7-1.2 mg ml^{-1} in arthritic joints [14, 42]. HA in normal SF is typically greater than 4 MDa in molecular weight but has also been reported to be 1.9 MDa [4, 5], and ranges between 0.3-0.7 MDa in joint injury or osteoarthritis [14].

Table 2.2 lists specific parameters used for each simulation. Simulations of normal and abnormal joints use the normal and pathologic ranges above, respectively, for equivalent pore size and HA molecular weight.

Solutions

Equation (1) was solved numerically using MATLAB 2010b (The MathWorks, Natick, MA) to obtain transient and steady-state concentration profiles and pressure drops across the layer. Equations (4) and (5) were used as boundary conditions for perfusion models (Simulations I and II), and Equations (5) and (6) were used as boundary conditions for physiological models (Simulations III and V). Results for Simulations III and IV are given for both the low and high ends of the pore size and HA MW ranges used.

The pressure drop across the layer and membrane, defined as the difference between the total pressure upstream of the membrane and that downstream, was estimated as the osmotic pressure across the membrane due to HA concentration at the membrane surface [21, 28, 54]. Thus, the pressure drop across the membrane was estimated as [21, 27]:

$$\Delta P(t) = \Pi_m(t) = b \cdot [c_{mem}(t)]^2 \qquad (14)$$

where the physicochemical parameter *b* is estimated based on solution properties of each simulation **(Table 1.1)**.

Total mass of HA upstream of the membrane over time was calculated by numerically integrating the concentration profile curves with respect to distance, and overall HA retention was calculated as the final mass upstream divided by the initial mass loaded. Results were compared with those from corresponding previous experimental and theoretical studies.

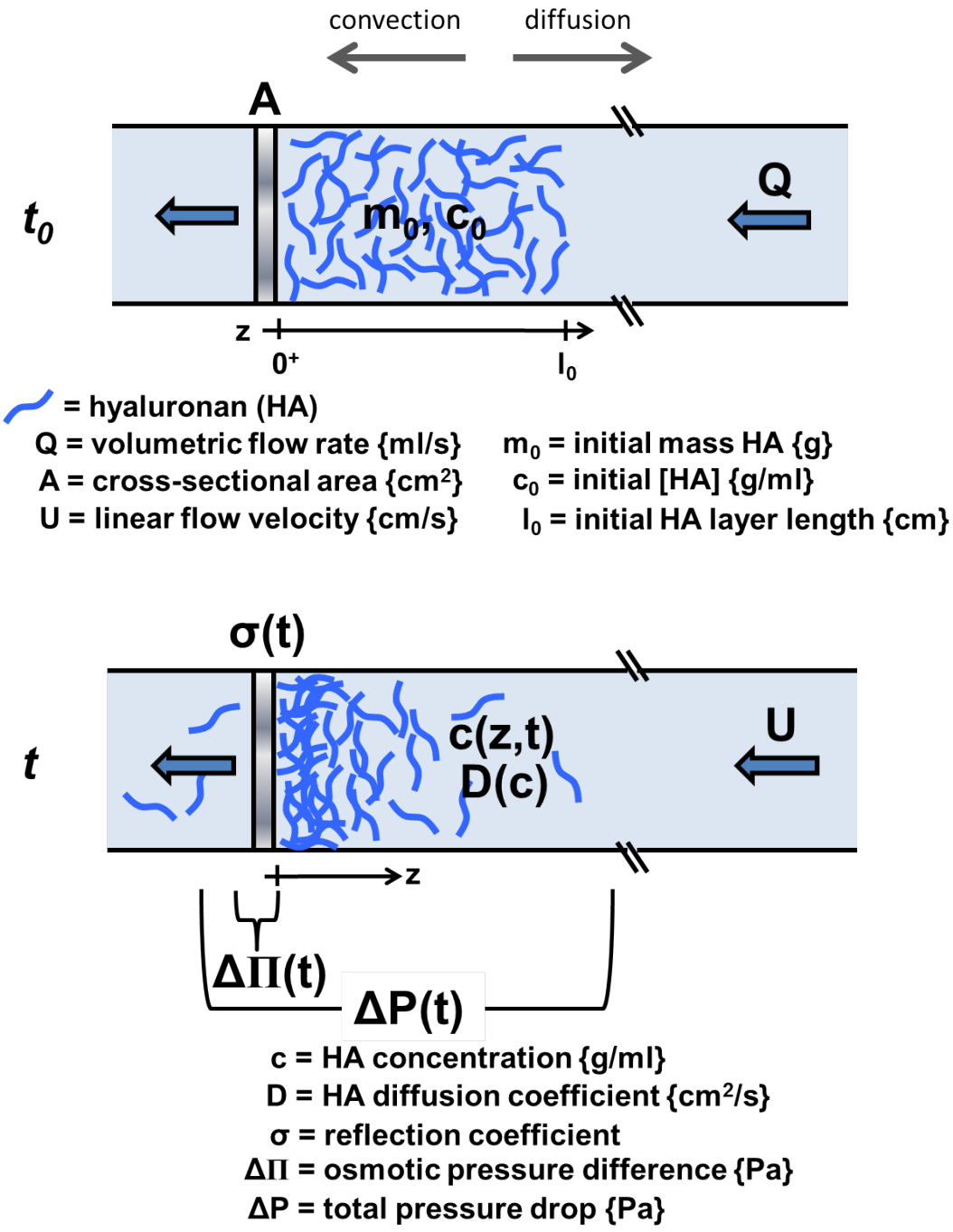

Figure 2.2: Ultrafiltration model of HA flow and concentration polarization at membrane surface, shown at initial time t_0 and intermediate time t. Solvent is perfused at velocity U through an initially uniform HA solution. HA passes through the membrane at fraction σ and diffuses according to D. The concentration gradient causes a pressure difference.

Table 2.1: List of model parameters and their units.

Variable	Units	Description
$c(z,t)$	g/ml	Concentration of HA
c_0	g/ml	Initial concentration of HA
$c_{mem}(t)$	g/ml	Concentration of HA at upstream membrane
t	s	Time
z	cm	Distance upstream from membrane
l_0	cm	Initial length of HA layer
Q	ml/s	Volumetric flow rate of solvent
A	cm^2	Cross-sectional flow area
U	cm/s	Linear flow velocity of solvent
D	cm^2/s	Diffusion coefficient of HA in solution
r_s	nm	Radius of solute
r_p	nm	Radius of membrane pore
ϕ		Partition coefficient of solute for membrane
σ		Reflection coefficient of solute for membrane
R_g	nm	Radius of gyration in solution
M	g/mol	Molecular weight
P	Pa	Hydrostatic pressure
μ	Pa·s	Dynamic viscosity of solvent
k	cm^2	Permeability
Π	Pa	Osmotic pressure
a	g/cm	Physicochemical parameter, permeability
m		Physicochemical parameter, permeability
b	$cm^6 \cdot Pa/g^2$	Physicochemical parameter, osmotic pressure

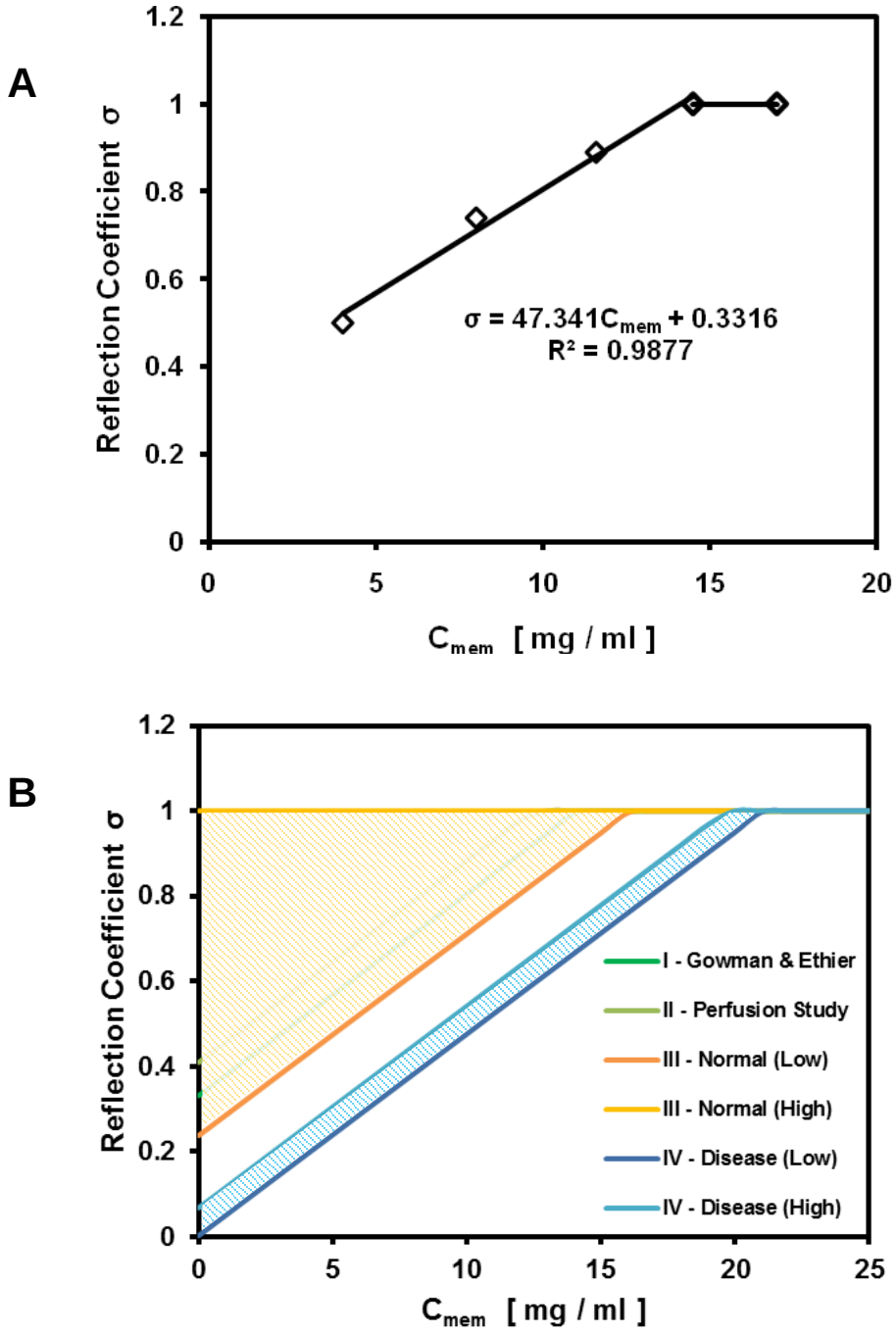

Figure 2.3: (A) Plot of concentration at membrane surface against measured reflection coefficient. Data is from Barry et al. [6]. **(B)** Estimated reflection coefficients as a function of membrane surface concentration for different simulation cases, using low and high ends of ranges of parameters. G&E: 434 kDa HA, 15 nm r_p. Perfusion study: 4 MDa HA, 50 nm r_p. Normal, low: 1.9 MDa HA, 45 nm r_p. Normal, high: 4 MDa, 15 nm. Disease, low: 0.3 MDa HA, 150 nm r_p. Disease, high: 0.7 MDa, 50 nm.

Table 2.2: Parameters used in model simulations.

Exp. No.	Initial HA [mg]	c_0 [mg/ml]	l_0 [cm]	Q [ml/s]	A [cm^2]	U [cm/s]	D [10^{-6} cm^2/s]	Source of Parameters
I	5.2	4.0	1.02	1.67×10^{-5}	1.27	1.31×10^{-5}	2.0	Gowman & Ethier
II	0.75	1.5	0.994	3.33×10^{-5}	0.503	6.63×10^{-5}	2.1	Previous exp.
III	4.0	4.0	0.00361	1.78×10^{-4}	277	6.44×10^{-7}	1.0	Physiol. (Normal)
IV	30	1.0	0.108	1.78×10^{-4}	277	6.44×10^{-7}	0.1	Physiol. (Disease)

2.4 Results

Theoretical Transient Profiles and Comparison to Experimental Data

Transient concentration profiles for all simulations largely followed similar shapes and trends. HA concentration at the membrane surface and pressure increased with time, usually to slowly plateau to steady-state values.

The approximate reflection coefficients of HA across the membrane were calculated as a function of membrane HA concentration **(Figure 2.3)**, and thus changed with time. The general form of the transient reflection coefficient corresponds to an initial loss of HA through the pores of the membrane followed by pore clogging and formation of a mesh of HA at the membrane surface, which further restricts passage of HA through the membrane. Thus, reflection coefficient increased linearly as total mass of HA upstream decreased with time; upon reaching a reflection coefficient of 1, the total retained mass also remained constant.

The data corresponding to experimental conditions used by Gowman and Ethier [21] show relatively rapid changes in concentrations and the pressure drop for the first 20 hours, followed by a slower leveling off to steady-state values between 20-40 hours **(Figure 2.4)**. The local maxima observed in the concentration gradient prediction **(Figure 2.4B)** corresponds to the inflection points seen in the concentration data. Plots of transient c_{mem} **(Figure 2.5A)** and ΔP **(Figure 2.5B)** show a smooth increases in membrane surface HA concentration and pressure drop with time, with slight bends in the curves at approximately 14 hours. Correspondingly, at this time, complete reflection was obtained and the reflection coefficient remained at $\sigma = 1$ for the remainder of the

simulation **(Figure 2.5C)**. Predicted transient concentration distributions **(Figure 2.6A)** and pressure **(Figure 2.6B)** were superimposed with those experimentally measured by Gowman and Ethier.

Transient data corresponding to conditions from experiments in Appendix A exhibit substantial changes in concentration in the first 4 hours of simulation, followed by a leveling off to steady-state values between 4-5 hours **(Figure 2.8A)**. At approximately 1.4 hours, the reflection coefficient reached a value of 1, corresponding to inflection points in the membrane concentration, pressure, and retained mass curves **(Figure 2.9)**. Concentrations near the membrane and pressure drop across the membrane increased at a greater rate following the transition to complete reflection. c_m increased at a rate of ~3 mg/ml per hour during the first hour of simulation, and ~11 mg/ml per hour from 1.5-3 hours. Similarly, predicted ΔP increased less than 2 kPa during the first hour, and more than 35 kPa during the next three hours, which was similar in overall time course shape but not value when compared with the pressure drop measured in Appendix A **(Figure 2.10)**.

Theoretical Steady-State Profiles and Comparison to Experimental Data

The final steady-state membrane surface concentration c_{mem}, total pressure drop ΔP, time until steady-state, and overall HA retention R for Simulations I and II are shown in **Figure 2.7** and **Figure 2.11**, respectively.

Simulations with parameters from experiments by Gowman and Ethier [21] (flow rate of 1.31×10^{-5} cm/s, diffusion coefficient of 2×10^{-6} cm^2/s, base reflection coefficient of 0.336, and initial HA mass of 5.2 mg) reached steady-state concentrations and pressure drops in approximately 40 hours, although concentration profiles appeared

nearly indistinguishable by 25 hours **(Figure 2.4A)**. At steady state, the concentration of HA at the upstream membrane surface was approximately 17.9 mg/ml, with the polymer concentration decreasing exponentially with distance upstream from the membrane until a distance of ~1 cm **(Figures 2.4A, 2.5A)**. The steady-state pressure drop across the membrane due to osmotic pressure was approximately 11.3 kPa, or 1.64 PSI, a 5.4-fold underestimate compared to that measured in the Gowman and Ethier study **(Figure 2.5B)**. After ~15 hours, the total mass of HA remaining upstream of the membrane reached a steady value of 3.6 mg, or 69% of the original mass loaded **(Figure 2.5C)**. Predicted steady-state values were compared with those experimentally measured by Gowman and Ethier **(Figure 2.7)**. Excellent agreement in steady-state membrane concentration, time to steady-state, and overall reflection coefficient were found.

Simulations of high MW HA flow through a 50 nm pore radius membrane at a flow rate of 6.62×10^{-5} cm/s, diffusion coefficient of 2.1×10^{-6} cm^2/s, base reflection coefficient of 0.41, and initial mass of 0.75 mg reached steady-state concentrations, concentration gradients, and pressure drops in approximately 5 hours **(Figures 2.8, 2.9)**. At steady-state, c_{mem} was 34.8 mg/ml, a 23-fold increase from the initial membrane surface concentration. The steady-state pressure drop across the membrane was 40.5 kPa, or 5.87 PSI. After ~1.5 hours, the total mass of HA remaining upstream of the membrane reached a steady value of 5.8 mg, or 78% of the original mass loaded **(Figure 2.9C)**. Comparisons between predicted and measured steady-state values **(Figure 2.11)** show that time until steady state and overall HA retention were reasonably consistent, however, the predicted pressure drop was an order of magnitude lower than that measured experimentally.

From the simulations and other validation simulations (not shown), it was verified that steady-state HA layer properties varied with initial mass of HA, solvent flow rate, HA diffusion coefficient, and reflection coefficient of HA through the membrane. Where steady-state was reached, increases in the mass of HA initially loaded or in solvent linear flow velocity U both resulted in a higher concentration of HA at the membrane surface and greater pressure drop across the layer at steady-state. Increases in reflection coefficients of HA, from either larger HA radius or smaller pore size, resulted in greater overall retention of HA upstream, larger concentrations of HA at the membrane surface, and greater pressure drops across the layer.

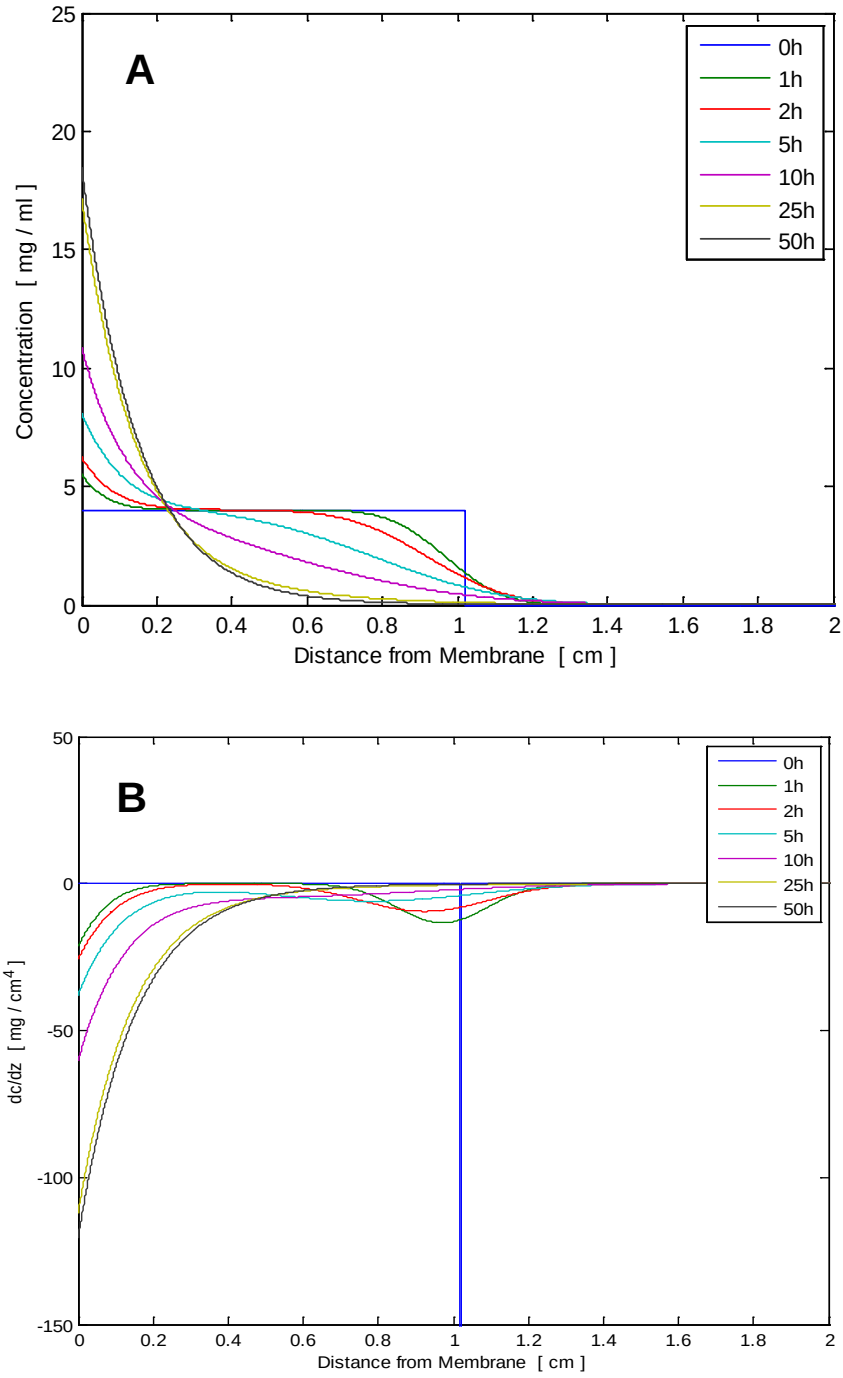

Figure 2.4: Theoretical (A) HA concentration profile and (B) concentration gradient for HA over time, for an initial mass of 5.2 mg HA, flow rate of 0.131 μm/s, and variable reflection coefficient. Simulation parameters correspond to those used in experiments by Gowman & Ethier.

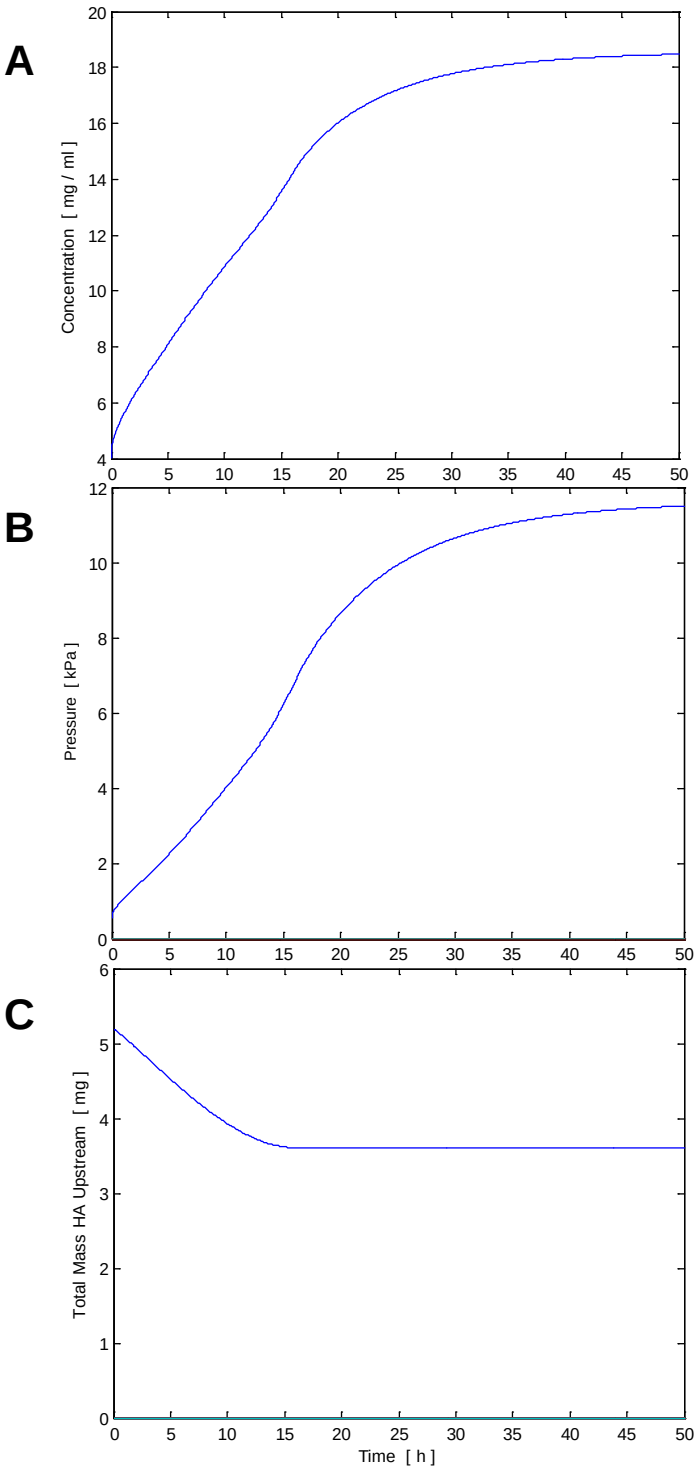

Figure 2.5: Simulated (A) transient membrane surface HA concentration, (B) total pressure drop, and (C) total mass of HA upstream. Simulation parameters correspond to those used in experiments by Gowman & Ethier.

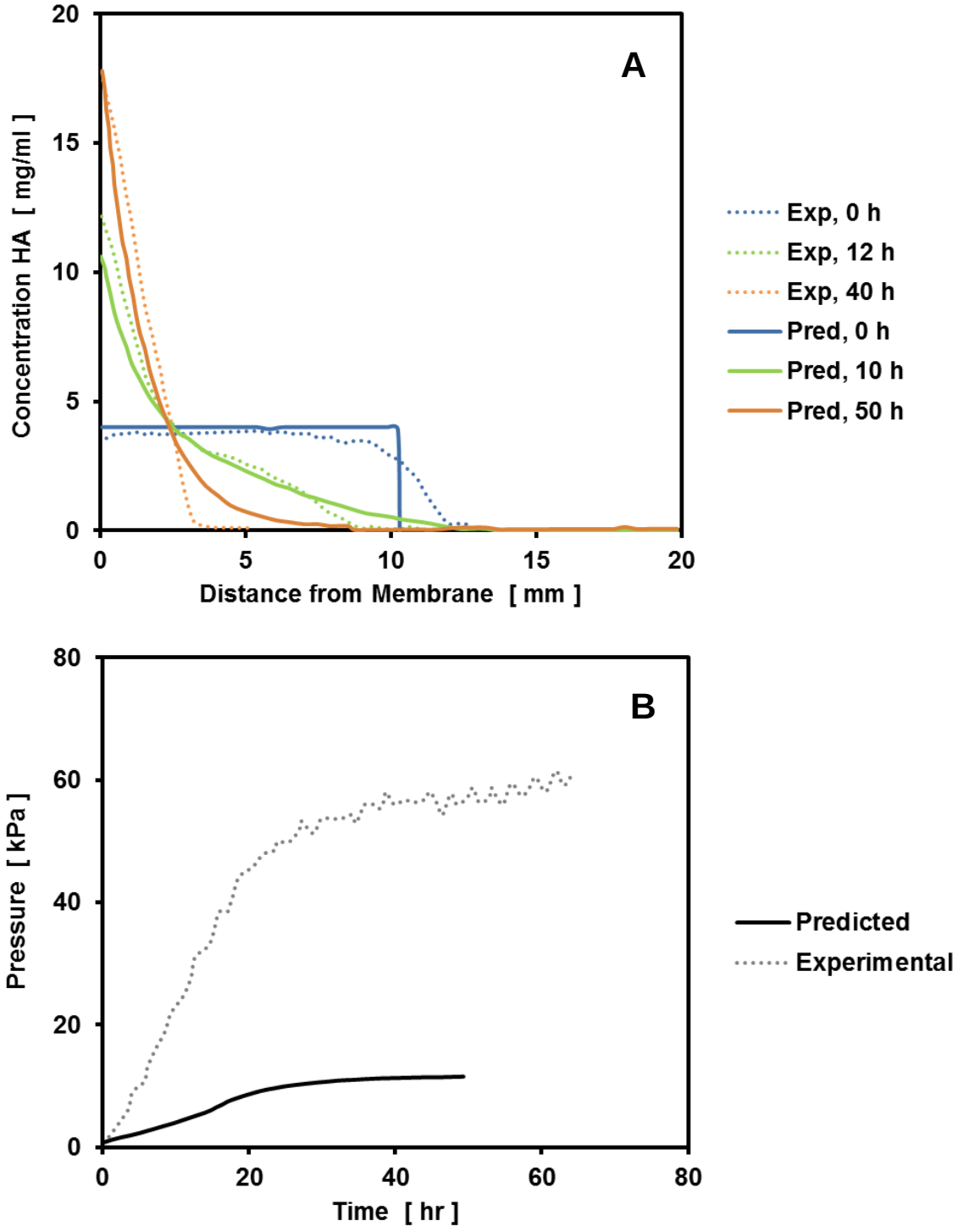

Figure 2.6: Comparison of (A) transient concentration distributions and (B) pressures predicted by the model and measured experimentally by Gowman and Ethier, n=1.

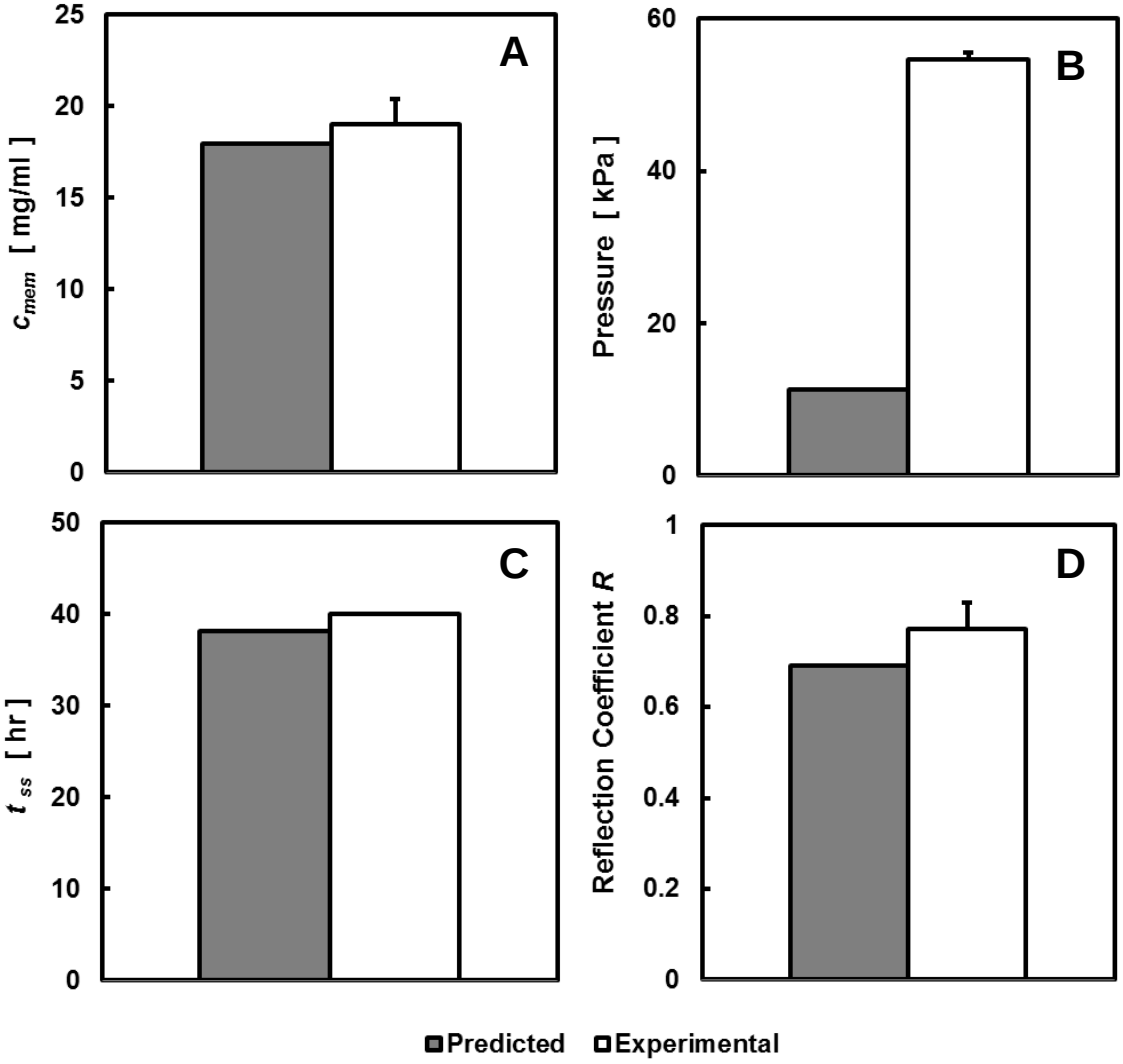

Figure 2.7: Comparison of predicted and reported experimental steady state (A) HA concentration at upstream membrane surface, (B) pressure drop across membrane, (C) time until steady-state, and (D) overall reflection coefficient. Parameters correspond to those used by Gowman and Ethier, n=2.

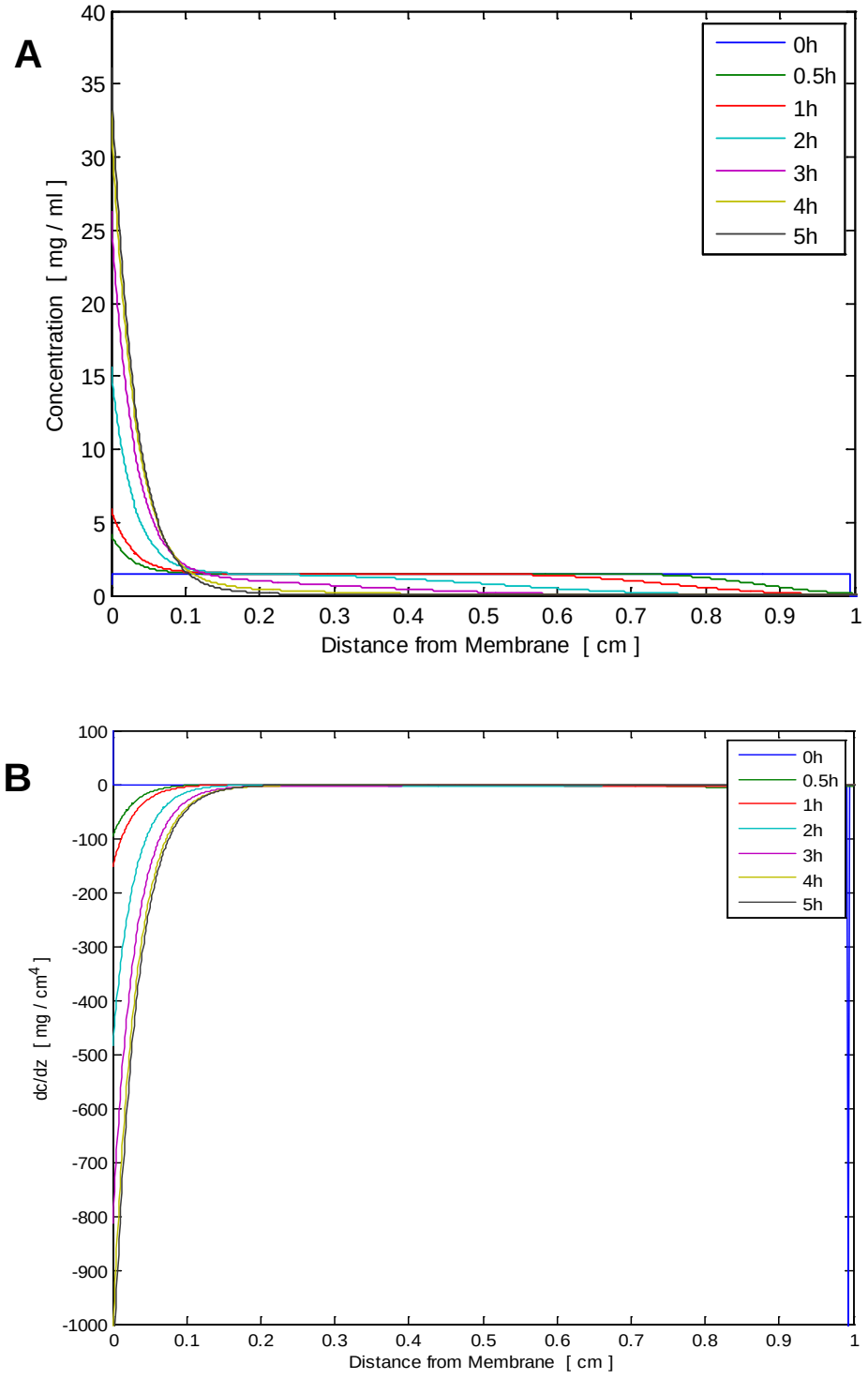

Figure 2.8: Theoretical (A) HA concentration profile and (B) concentration gradient for HA over time, for an initial mass of 0.75 mg HA, flow rate of 0.662 µm/s, and variable reflection coefficient. Simulation parameters correspond to those used in experiments in Appendix A.

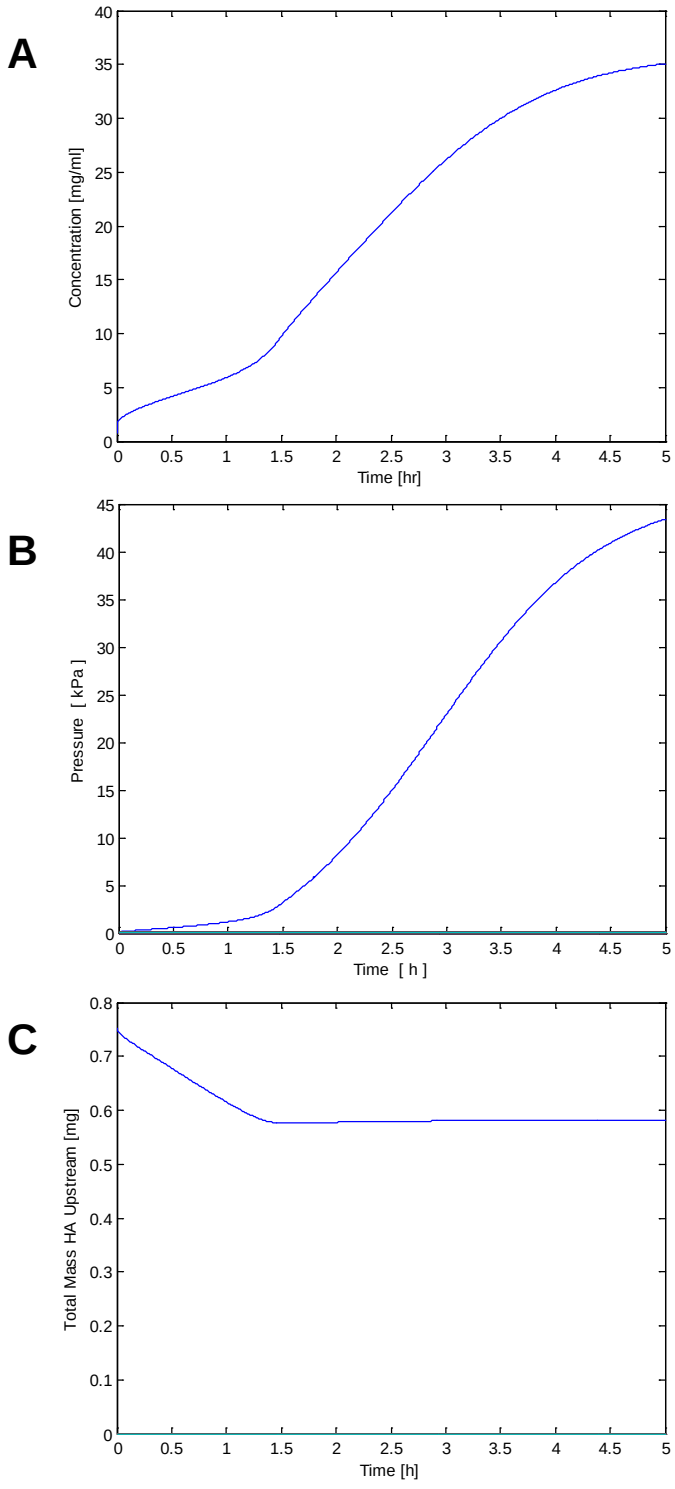

Figure 2.9: Simulated (A) transient membrane surface HA concentration, (B) total pressure drop, and (C) total mass of HA upstream. Simulation parameters correspond to those used in experiments in Appendix A.

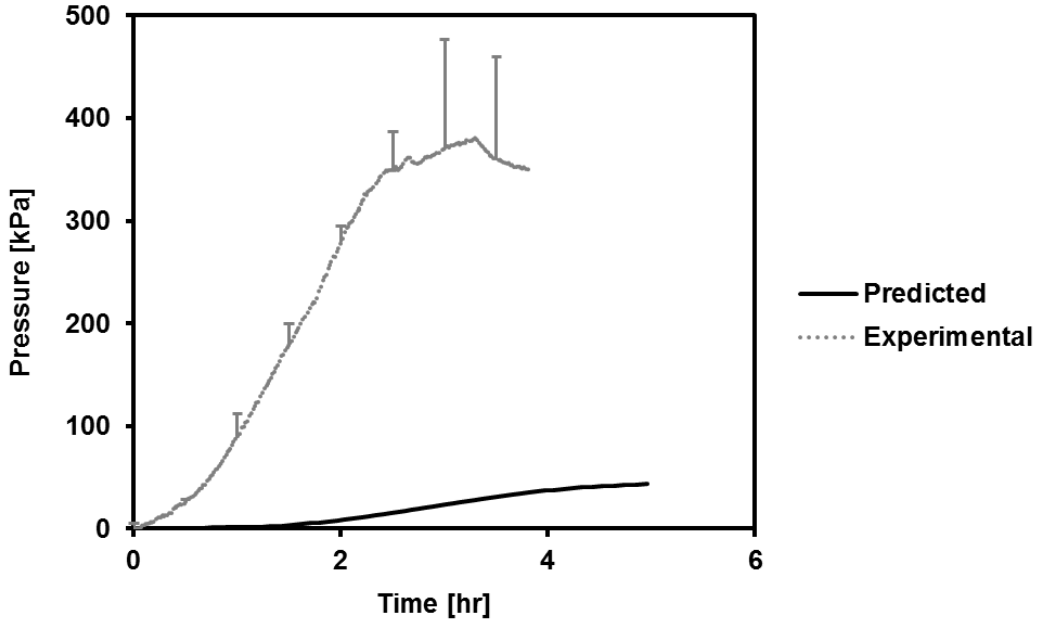

Figure 2.10: Comparison of pressure drop over time predicted by the model and measured experimentally (n=3) in Appendix A. Pressure drop was estimated in the model as the osmotic pressure across the membrane due to c_{mem}.

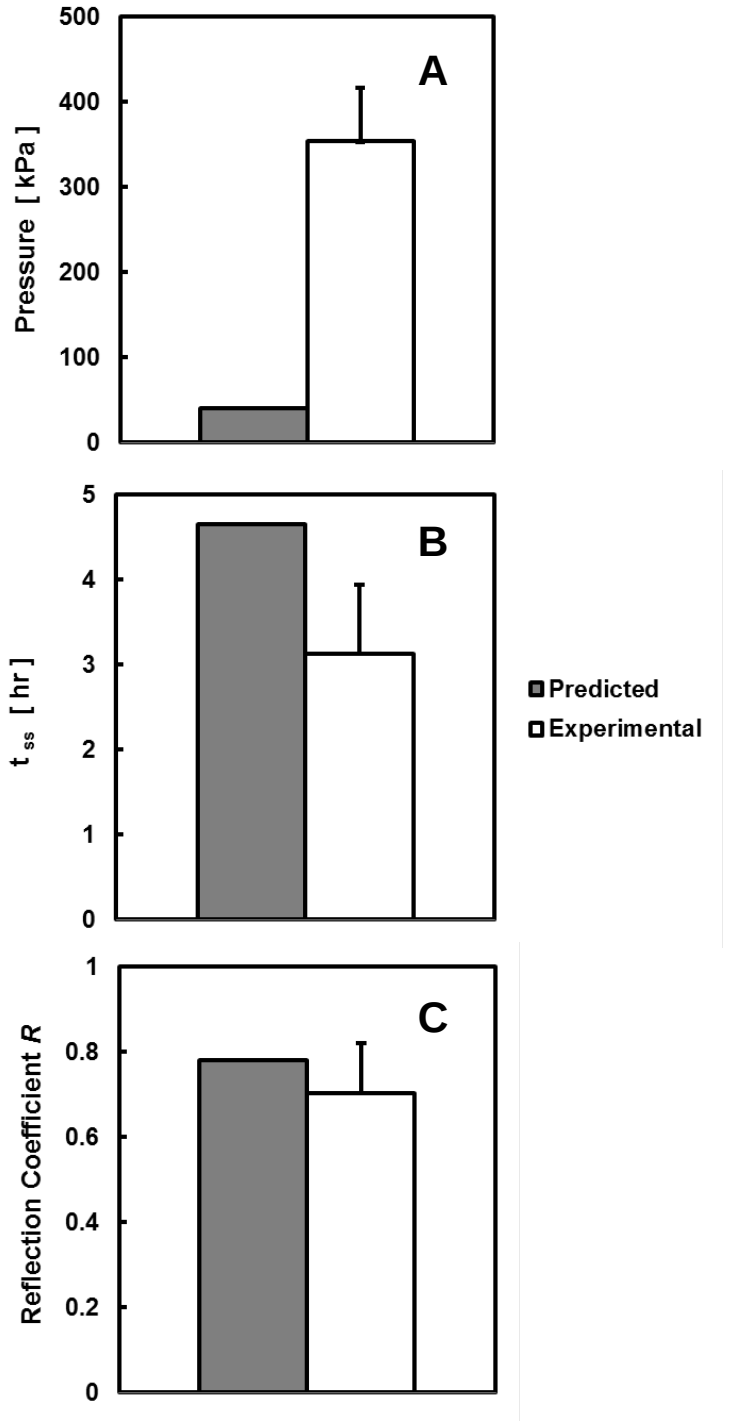

Figure 2.11. Comparison of predicted and experimental steady state (A) pressure drop across membrane, (B) time until steady-state, and (C) overall reflection coefficient. Parameters correspond to those used in Appendix A, n=3.

Theoretical Simulations of the Normal Knee Joint

A range of molecular weights for normal human SF HA, from 1.9-4 MDa [14] was used to estimate the transient reflection coefficient. For the high end of the range of estimates (2.7-4 MDa HA, 15 nm pore size), flow in normal human knee joints was predicted to result in a small steady-state build-up of HA at the upstream membrane surface with perfect retention of HA in the joint space **(Figure 2.12A)**. At steady-state, the HA concentration at the upstream membrane surface increased to 4.003 mg/ml and the pressure across the membrane was ~4.14 mmHg (0.552 kPa) **(Figure 2.14)**. Steady-state was obtained between 6-11 seconds, such that no difference could be detected in the concentration and concentration gradient date **(Figure 2.12A, 2.13A)**, and all HA was retained upstream of the membrane. For the low estimates (1.9 MDa HA, 45 nm pore size), an initial build-up of HA at the membrane surface occurred in the first few seconds **(Figure 2.12B)**, followed by a decrease in HA concentration as the molecules passed through the membrane **(Figure 2.14)**. The local maximums in the concentration gradient predictions **(Figure 2.13)** at 0.1 s and 0.5 s correspond to the inflection points observed in the concentration data **(Figure 2.12)**.

Theoretical Simulations of the Pathologic Knee Joint

Simulations of physiological human knee joints in disease, such as osteoarthritis, and acute injury showed a negligible initial build-up of HA at the membrane surface, followed by a steady decrease in concentration as the HA was carried through the membrane **(Figure 2.15, 2.16)**. HA in OA, RA, and joint injury is of lower molecular weight, ranging between 0.3-0.7 MDa [14], and effective membrane pore sizes are greater due to tissue degradation, assumed to be approximately 50-150 nm in radius.

The estimated transient reflection coefficient was low at both ends of this range **(Figure 2.3B)**, leading to an overall 67% loss of HA from the joint space within 13 hours, as shown in **Figure 2.17**. Unlike simulations of the normal knee joint, concentrations decreased to zero over time. Concentration at the upstream membrane surface rose to up to 1.02 mg/ml over the first 2 hours of simulation time, and then dropped to less than 0.04 mg/ml by 50 hours. Likewise, intra-articular pressure due to osmotic pressure across the membrane reached a maximum of 43 Pa (0.32 mmHg) before decreasing to zero.

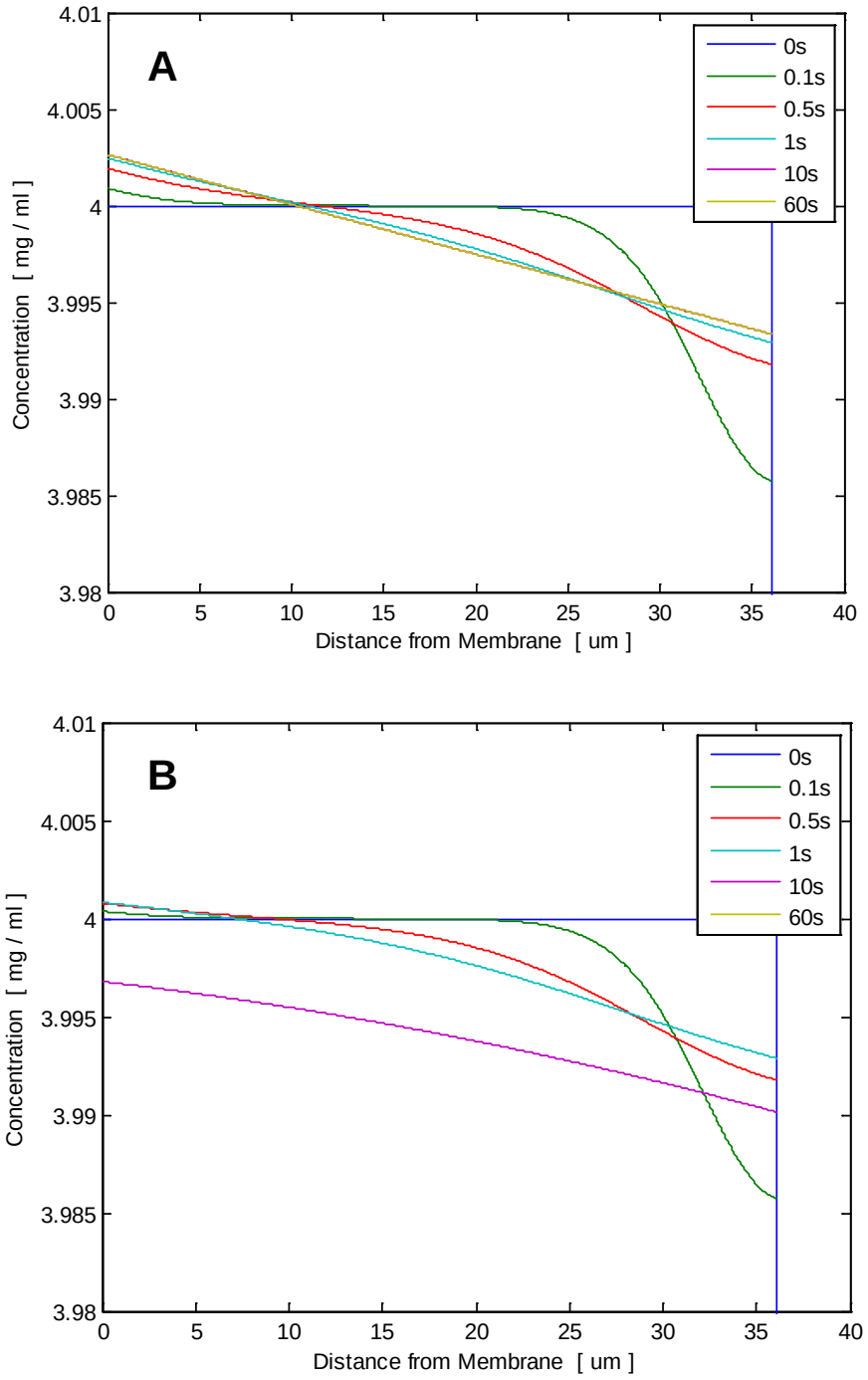

Figure 2.12: Theoretical HA concentration profile over time, for an initial mass of 4 mg HA, flow rate of 0.00644 µm/s, and variable reflection coefficient. Simulation parameters correspond to the (A) high and (B) low ends of the range of values reported for a normal human knee joint. Low: 1.9 MDa HA, 45 nm r_p. High: 4 MDa, 15 nm.

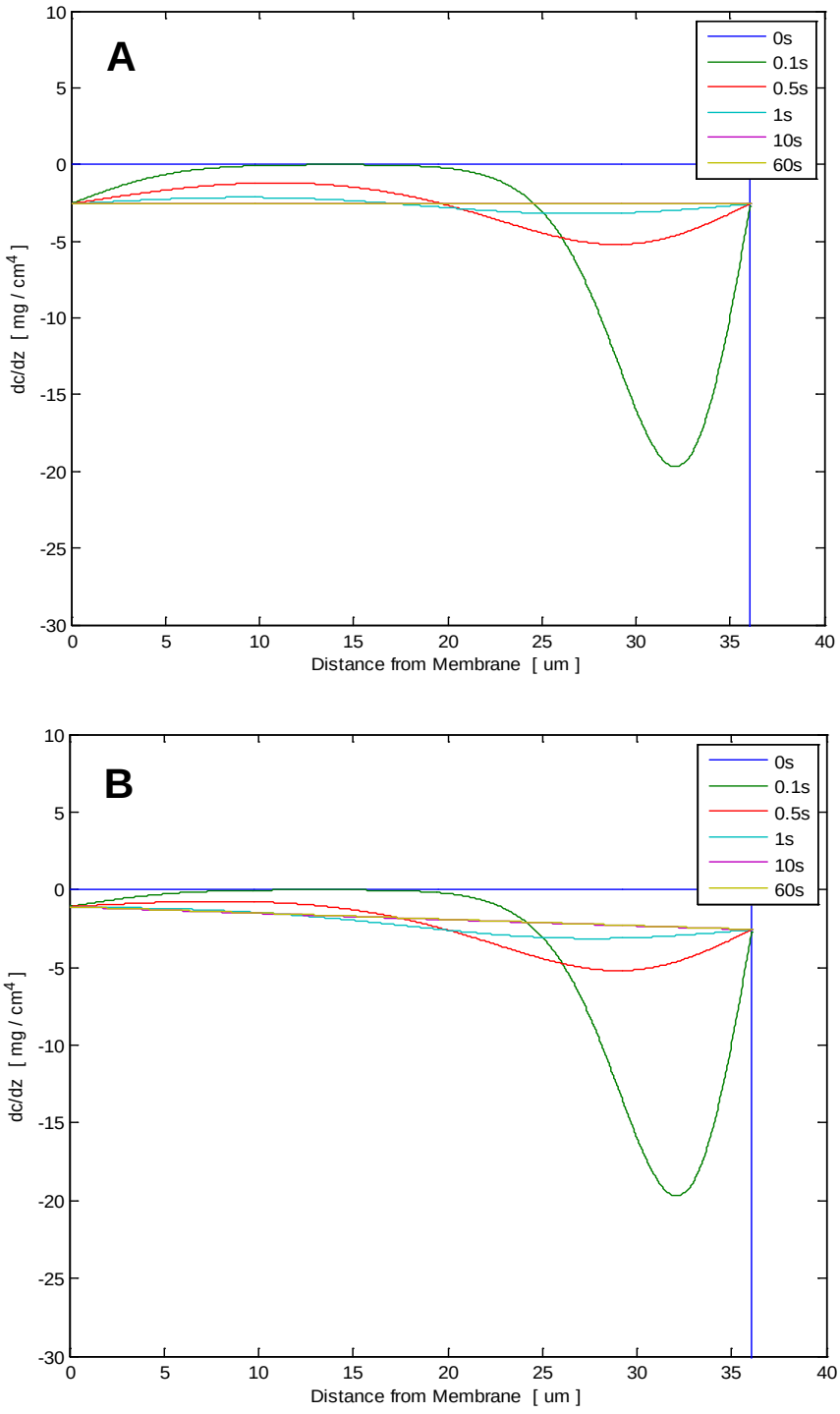

Figure 2.13: Theoretical concentration gradient of HA over time, for an initial mass of 4 mg HA, flow rate of 0.00644 µm/s, and variable reflection coefficient. Simulation parameters correspond to the (A) high and (B) low ends of the range of values reported for a normal human knee joint. Low: 1.9 MDa HA, 45 nm r_p. High: 4 MDa, 15 nm.

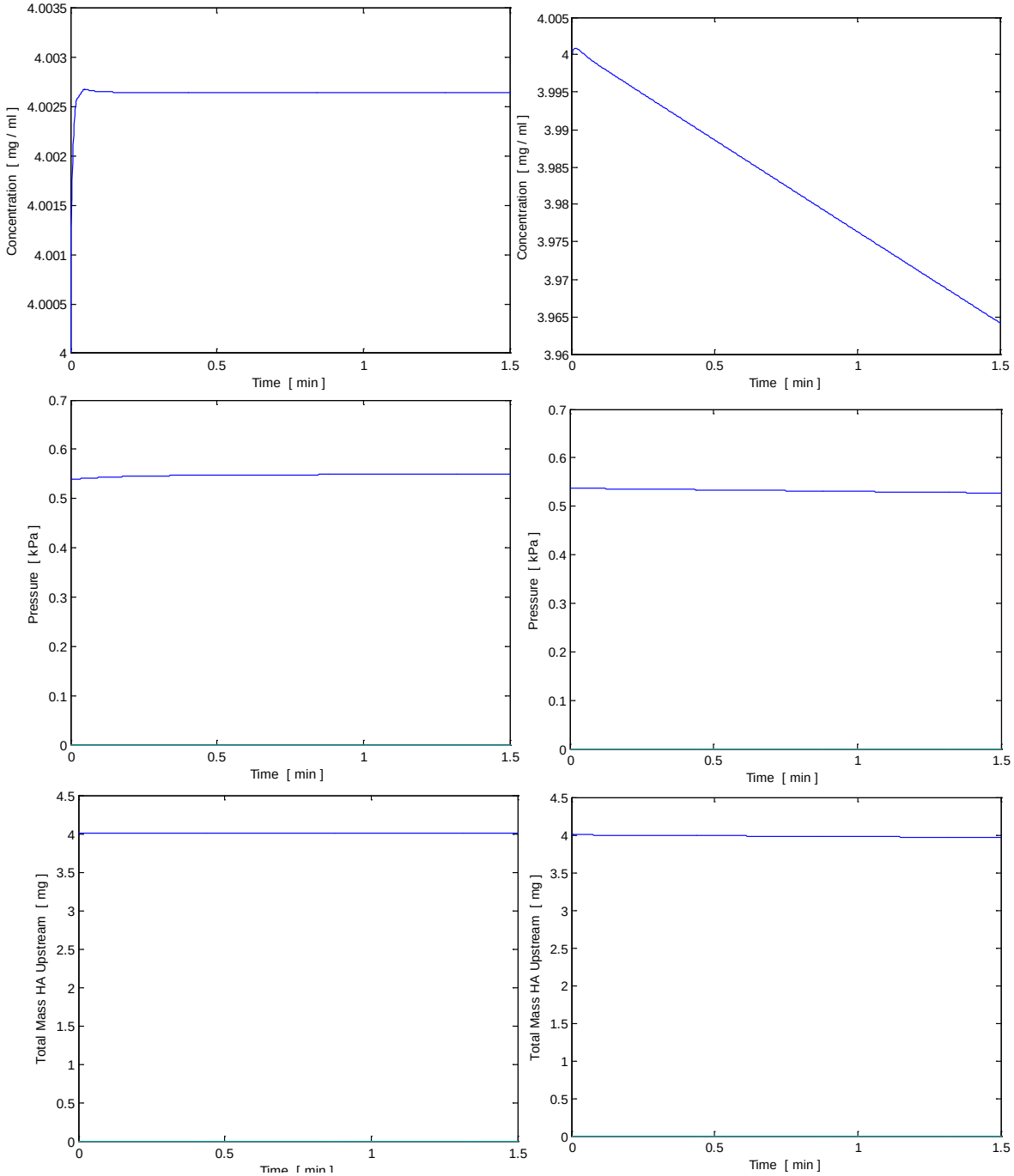

Figure 2.14: Theoretical transient HA c_{mem}, pressure drop, and mass upstream, for an initial mass of 4 mg HA, flow rate of 0.00644 µm/s, and variable reflection coefficient. Simulation parameters correspond to the high and low values reported for a normal human knee joint. Low: 1.9 MDa HA, 45 nm r_p. High: 4 MDa, 15 nm.

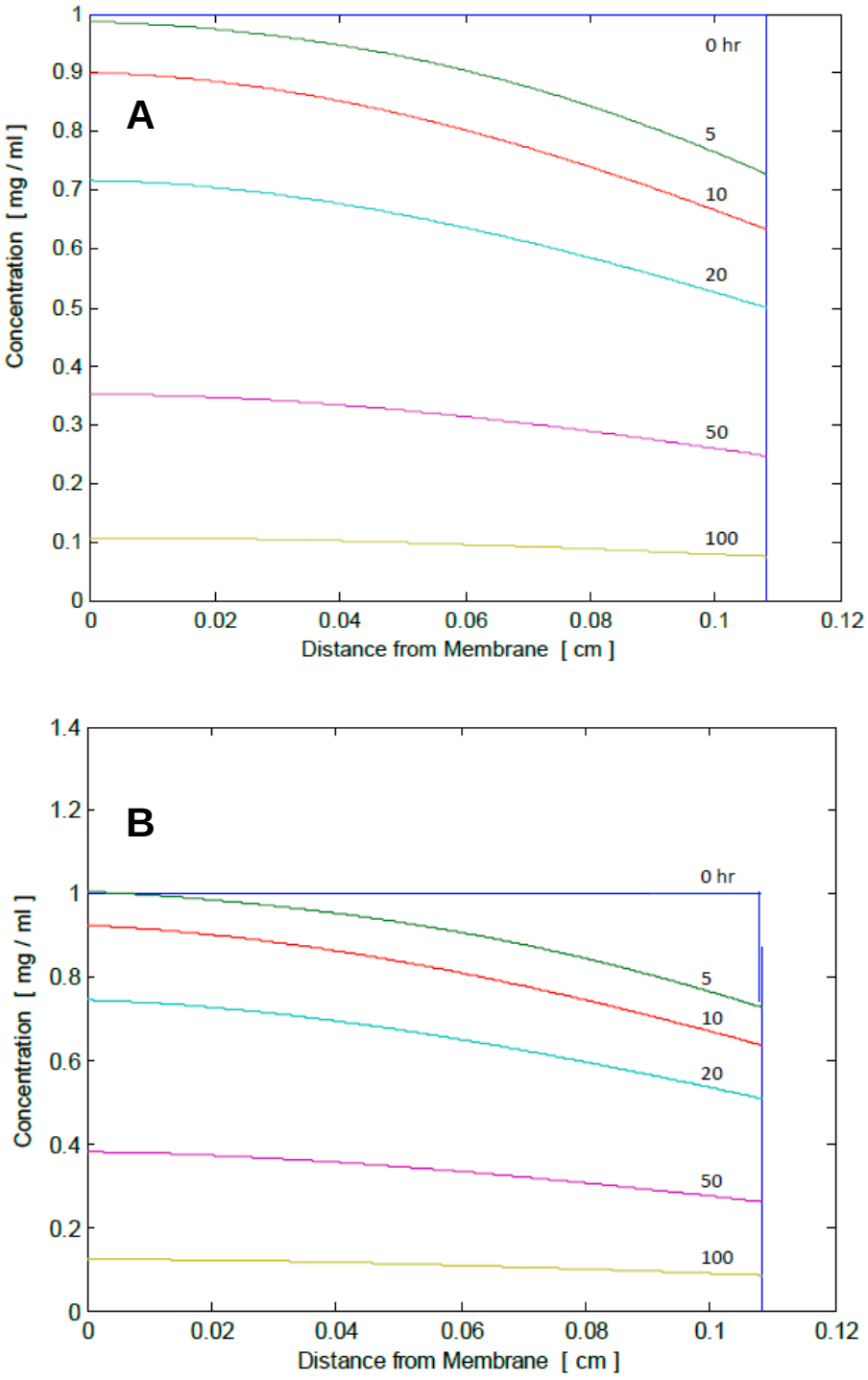

Figure 2.15: Theoretical HA concentration profile over time, for an initial mass of 30 mg HA, flow rate of 0.0208 μm/s, and variable reflection coefficient. Simulation parameters correspond to the (A) low, and (B) high, values reported for a diseased human knee joint. Low: 0.3 MDa HA, 150 nm r_p. High: 0.7 MDa, 50 nm.

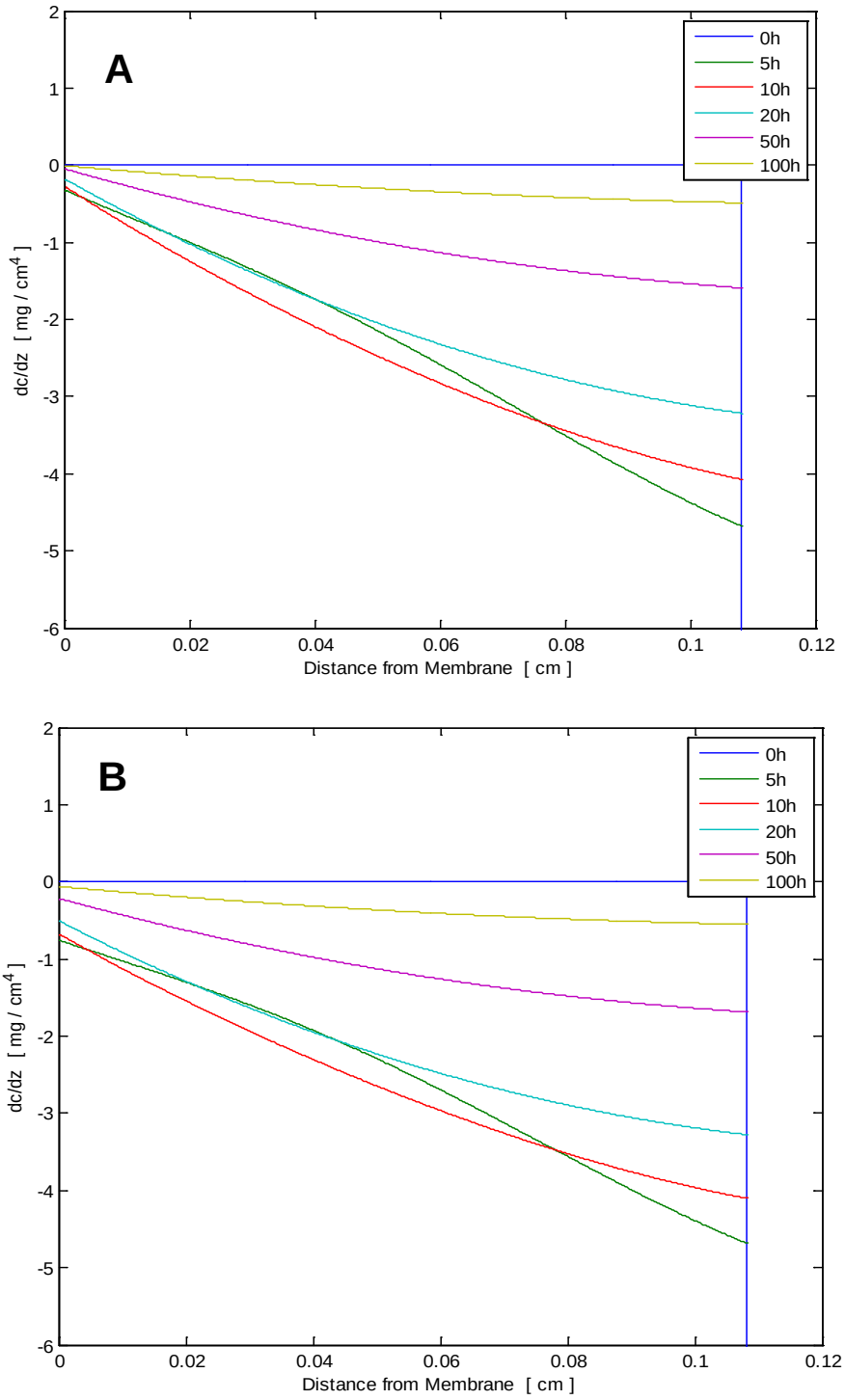

Figure 2.16: Theoretical concentration gradient for HA over time, for an initial mass of 30 mg HA, flow rate of 0.0208 µm/s, and variable reflection coefficient. Simulation parameters correspond to the (A) low, and (B) high, values reported for a diseased human knee joint. Low: 0.3 MDa HA, 150 nm r_p. High: 0.7 MDa, 50 nm.

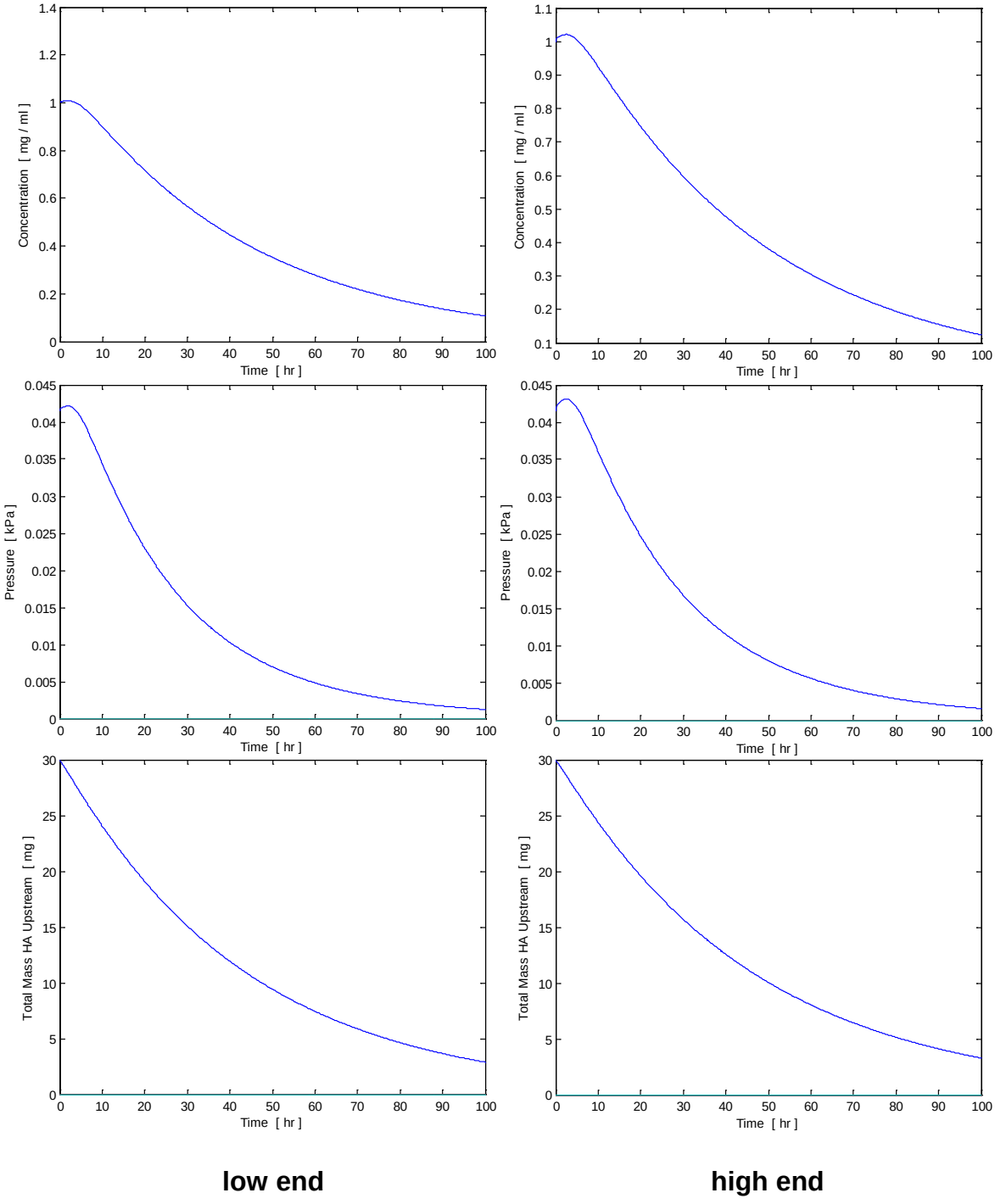

Figure 2.17: Theoretical (A) transient HA c_{mem}, (B) pressure drop, and (C) mass upstream, for an initial mass of 30 mg HA, flow rate of 0.0208 μm/s, and variable reflection coefficient. Simulation parameters correspond to those reported for a diseased human knee joint. Low: 0.3 MDa HA, 150 nm r_p. High: 0.7 MDa, 50 nm.

2.5 Discussion

Steady-state and transient HA concentration distributions and total pressure drops across concentration polarization layers were investigated theoretically and experimentally using various parameters. An approximate expression for a variable reflection coefficient as a function of membrane surface concentration **(Figure 2.3B)** was applied to a numerical convection-diffusion model for flow through an HA solution. Effects of initial HA content, solvent flow rate, and reflection coefficient were assessed using the model and compared to previous theoretical and experimental studies **(Figures 2.4-2.11)**. SF and joint parameters were then used to predict HA concentration profiles and retention in health and disease **(Figures 2.12-2.17)**.

Limitations of the Model

Several assumptions and simplifications made in this model may affect predictions relative to experimental data and physiological conditions. Convection was modeled as uni-directional flow, rather than as flow in a capsule. Metabolic factors such as HA secretion and degradation were not accounted for in the present model, such that the total cumulative mass of HA both upstream and downstream of the membrane remained constant at the mass initially loaded. These factors are expected to affect HA convection and concentration in the in vivo joint, although they are less applicable in simulations of ultrafiltration studies through a semi-permeable membrane.

The value of the reflection coefficient over time was modified from experimental retention measurements from Barry et al. [6] with alterations for differences in HA molecular weight and membrane pore size, and are therefore not

exact. The reflection coefficient of HA through the membrane at any point in time is influenced by multiple factors, including the original pore size of the membrane, the effective radius of the solute, molecule-molecule interactions, and interactions between HA and the membrane such as pore fouling or adhesion. These effects were taken into account on a general macroscopic level using experimental reflection coefficient measurements made by Barry et al. [6]. It was assumed that the base reflection coefficient, that is, the reflection coefficient for HA in a dilute (un-entangled) solution, was dependent solely on the size of the HA molecule and the membrane pore size. Using values from Barry et al., the base reflection coefficient was modified for the different simulations, with greater reflection coefficients for HA of higher MW and for membranes of smaller pore size. It was also assumed that the reflection coefficient would increase similarly with membrane surface concentration c_{mem} for all cases, such that the relationship between σ and c_{mem} found in Barry et al.'s study could be applied to the other cases as well. This estimation suggests that perfect reflection ($\sigma = 1$) is obtained at lower membrane HA concentrations for larger HA and membranes with smaller pore sizes, which is a reasonable assumption. Furthermore, total retained fractions at steady-state for the simulations correspond reasonably well to previously reported experimental values for loss of HA during filtration **(Figures 2.7D, 2.11C)**. Thus, although values for the reflection coefficient may not be exact, the approximation used in this model are good indicators of trends in HA loss through the membrane over time. For improved characterization, however, the relationship between the increase in transient reflection coefficient with HA concentration, could be modeled as a function

of HA properties, membrane characteristics, and filtration rate, rather than generalizing the relationship observed in Barry et al. to all simulations.

The diffusion coefficient of HA was estimated as a constant bulk value, rather than as a function of HA concentration. Differences between predictions and experimental results may have occurred due to imperfect simulation of the diffusion coefficient of HA in solution, which varies with concentration [6, 67] and has not been reported for HA solutions greater than 20 mg/ml in concentration [6]. In this model, the diffusion coefficient was simplified to a constant value to prevent oscillations in the solutions at low diffusion coefficients. The values used for each case were adjusted to correspond to intermediate-high concentrations within the range of concentrations present in the HA layer to better reflect diffusion effects, especially near the membrane. They are therefore slight underestimates of diffusion near the surface of the membrane and overestimates of diffusion further from the membrane. Thus, with a concentration-dependent diffusion coefficient, we may expect there to be greater back-diffusion near the membrane and less back-diffusion near the lagging edge of the HA layer, leading to a lower c_{mem} as well as a smaller final polymer layer length l_f than those obtained using the present model. Because diffusion is a slower process than convection in this process, it is important for future expansion of the project to improve the accuracy of the model by considering the concentration dependence of HA diffusivity.

There are a number of other factors that may affect fluid and HA retention during physiological scenarios. For example, flexion of the synovial joint may alter the synovium during that time period, leading to temporary changes in membrane pore size or thickness. Furthermore, these changes may be unevenly distributed across the

synovium, which might affect the effective flow area. For example, stretching of one region of the synovium may lead to a greater pore size in that region, while simultaneous compression of a different region may lead to decreased pore size. Mechanical stimuli of the synovial joint structures, such as the stretching of synovium, can also alter secretion of HA by synoviocytes [47], thus making the mass of HA available variable with time.

Finally, although the model assumes that the total pressure drop can be estimated using the osmotic pressure due to the concentration of HA at the membrane surface, it is likely that pore occlusion also contributes significantly to an increase in flow resistance and the measured pressure drop across the membrane, and may be an important source of error in this study's pressure drop estimations. Although we may assume that membrane pores are clear at the start of filtration, during filtration, some pores may become irreversibly occluded. As the membrane collects solute particles with increased filtration, the effective pore radius r_p decreases and the number of pores decreases. These effects both cause an increase in the pressure drop across the membrane. Expansion of the model to include the pressure drop due to pore clogging requires use of Darcy's Law, as well as an estimate of the proportion of clogged pores through a stochastic analysis[33].

Comparison of Theoretical Model to Experimental Data

Comparison of results with experimental data from Gowman and Ethier [21] shows general agreement between the experimental measurements and theoretical predictions of mass changes in the concentration polarization process **(Figures 2.6, 2.7)**. Theoretical and experimental transient concentration distributions **(Figure 2.6)** are

similar at all time points. Differences near the lagging edge of the profile are likely due to the fixed diffusion coefficient in the model, which overestimates back-diffusion at further distances from the membrane. HA concentration at the upstream membrane surface reached a steady-state value of ~18 mg/ml by 40 hours; measurements obtained experimentally by Gowman and Ethier for the same initial set-up also show a steady-state HA membrane surface concentration of ~18 mg/ml, and the authors established that steady-state was reached by 40 hours.

Gowman and Ethier also integrated their experimental concentration profiles with respect to position to obtain the total mass of HA in the flow cell, and concluded that between 18-29% off the initial mass was lost during the experiment, mostly during the first 10-20 hours. The model in this study predicted a 31% loss of initial HA mass in the first 15 hours, with no additional loss thereafter. Differences may be due to polymer-polymer or polymer-membrane interactions or the inhomogeneity of experimental HA solutions (e.g. molecular weight distributions), however, the value and timeframe of the overall polymer retention predicted by the model are in general agreement with the reported data.

Gowman and Ethier measured a steady-state pressure drop of between 450-470 mmHg, compared to the predicted value of 84.8 mmHg. This 5.4-fold underestimate may be due to the specific physicochemical parameters used to estimate the osmotic pressure across the membrane, which vary with solvent type, ionic strength, pH, temperature, impurities, and polymer MW distribution. Furthermore, pore occlusion by HA was likely to occur, and thus may contribute to experimental resistances. To obtain a predicted pressure drop similar to that measured, an HA membrane surface

concentration of 40.4 mg/ml would be required, or else a value of 1.70×10^9 for the physicochemical parameter *b* used in Equation (14), compared to the value of $b = 3.34 \times 10^8$ that was used in the model. The required physicochemical parameters are reasonably close to those reported in **Table 1.1** and used in the study, and are thus a possible source of error contributing to the difference between predicted and measured pressure drop.

HA concentration distribution results were generally consistent with those observed in a previous HA solution perfusion study **(**Appendix A, **Figure 2.11)**. Pressure measurements obtained experimentally ranged between 45-60 PSI (310-414 kPa), which are greater than the predicted 40.5 kPa osmotic pressure drop across the membrane. Similar issues with physicochemical parameters and membrane occlusion are likely to be applicable here as well. Perfusion experiments in Appendix A appeared to approach steady-state pressures by 4 hours, and the model predicted that the time to steady state was 4.7 hours. Finally, the model predicted overall retention of 78% of the initial HA, which corresponds relatively well with the experimental samples assayed upstream and downstream from the membrane, which showed overall HA retention of approximately 70 ± 12% (Appendix A). Differences may be due to the preparation of the HA solutions used in the perfusion study, and the degradation of the high MW HA over time. Gowman and Ethier have also suggested that commercially-available membrane filters have an inconsistent distribution of pore sizes [21]; the track-etched membranes used in the corresponding experiments in Appendix A are reported by the manufacturer to have a typical intra-lot variation in pore size between 2-3%.

Applications to the Physiologic and Pathologic Joint

Application of physiological parameters for human knee joints, in both health and disease, to the model reveals important differences in the transport of HA and fluid from the joint capsule. Disregarding metabolic processes and normal enzymatic degradation of molecules, much of the HA present in the joint capsule remains contained within the synovial membrane in a normal joint. Within a normal distribution of HA in SF, it is assumed that the higher MW HA (4 MDa), corresponding to the high end of predictions, will have a larger contribution to resistance and the state of the joint. The high MW of HA in normal SF, along with the pore properties of healthy synovial joint tissues (i.e. synovium, articular cartilage), leads to selective molecular sieving of HA by the synovial membrane, which retains HA while allowing fluid to pass through. Steady-state is obtained rapidly, within the first 11 seconds, such that transsynovial permeability is relatively constant with time, even in sustained flow. The predicted pressure drop of 4.14 mmHg is similar in magnitude to intra-articular pressure measurements reported in literature. McDonald and Levick [45] found that pressures of 13.2-14.7 mmHg corresponded to flow of ~25 µl/min of 6 mg/ml HA in rabbits, and Nade and Newbold [50] measured intra-articular pressures of between 7-42 mmHg in dog knees, depending on the position of the knee. Predictions of osmotic pressure were again made using the second-order power law equation and estimated physicochemical parameters, and were thus again subject to differences based on specifics of the solution.

In contrast, results simulating the joint in disease or injury are markedly different in their transient behaviors, and reach steady-state only by the depletion of HA from the joint space. As observed in simulations of the normal joint, those of the arthritic or injured joint show a slight increase in HA concentration at the membrane surface

concentration initially, however, concentrations at the membrane and across the entire upstream length drop dramatically with sustained flow. This suggests that during transient motion of the joint, some degree of transsynovial molecular sieving does occur, leading to a small amount of outflow resistance. However, after the first 2 hours of sustained flexion, hydraulic resistance decreases as all remaining HA is lost through the membrane. While a large proportion of HA is continuously retained in the ideal normal joint modeled, the majority is lost from the arthritic model by 10 hours and must be replenished. Overall, although SF in osteoarthritis and injury often contains more HA by mass, its larger fluid volume and lower HA MW, in conjunction with greater pore sizes in joint tissues, lead to a decreased ability to form an HA concentration polarized layer against the inner membrane surface and subsequent increases in HA and fluid permeability.

Conclusions

From the results, we may come to several conclusions regarding the concentration polarization of HA, its effects on transsynovial flow in the synovial joint, and how this process may be altered in injury and disease. The concentration polarization of HA, which occurs as a result of selective retention of HA in the joint space, decreases hydraulic conductance and maintains SF composition in the synovial joint. The formation of a concentrated polymer network at the inner membrane surface may also decrease the efflux of additional HA or other SF proteins (albumin, regulatory cytokines, etc.) from the joint. Compromising of this mechanism due to cleavage of HA chains, dilution of SF, or degradation of joint tissues, as observed in OA and joint

injury, may lead to fluid depressurization and loss of important SF molecules, causing further damage to the synovial joint.

Using the mathematical model in this study, we have been able to examine the process of concentration polarization of HA. The poor agreement between theoretical and experimental pressure may be able to be resolved with expansion of the model to consider the additional resistance contributed by pore occlusion during filtration. Further refinement of the model could include addressing the concentration dependence of HA diffusivity, improvement of the accuracy of transient HA reflection modeling, and the use and validation of more applicable physicochemical data. However, the overall agreement in concentration distributions and other transient and steady-state values, such as the time to reach steady state and the total HA retention, suggests that with additional work on its robustness, this model may be useful in examining effects of changes in HA solution composition, membrane characteristics, and other parameters on the filtration of HA. With expansion and validation of the preliminary model, it may serve as a basic framework for predicting macromolecular flow and concentration polarization for in vitro and in vivo convective-diffusive studies. If with the expanded model, similar differences in permeability are found between simulations using normal and diseased synovial joint parameters as those findings in this study, the results may have implications for the study of the progression and treatment of joint injury and disease.

2.6 Acknowledgments

The thesis author is the primary investigator and thanks co-authors William McCarty and Dr. Robert Sah for their contributions.

CHAPTER 3

CONCLUSIONS

3.1 Summary of Findings

The objectives of this work were to (1) expand and solve a mathematical model to analyze HA concentration polarization, including steady-state and transient concentration profiles and pressure drops, (2) to assess the validity of the model by comparison with other experimental and theoretical studies, and (3) to apply the model to physiological situations in which HA composition and retention are altered. The results from this study provide an additional understanding of HA concentration polarization, its effects on transsynovial flow in the synovial joint, and how this process may be altered with changes in HA concentration and reflection.

In Chapter 2, a mathematical ultrafiltration model was solved numerically to evaluate the dynamics and steady-state properties of HA molecular sieving and concentration polarization in health and disease. Validation using experimentally reported parameters showed general agreement in transient and steady-state concentration distributions and retention of HA, although estimations of the pressure drop across the membrane and layer were underestimated in the model. In this model, HA retention, joint space HA concentration distribution, steady-state time scales, and dynamic hydraulic permeability were predicted to be altered with decreased initial HA concentration and molecular weight.

3.2 Directions for Future Work

The current work can be expanded in the future in a number of ways, including an extension of the mathematical model to include additional parameters and processes in the synovial joint, and further in vitro testing of HA and SF filtration through semi-permeable membranes or tissue.

Although the model in this study is a reasonable preliminary characterization of dynamic HA concentration polarization and retention during filtration, important next steps involve expansion of the model to consider resistance contributions from pore occlusion, the concentration dependence of HA diffusivity, and improvement of the transient reflection coefficient estimation. The model could also be extended by incorporating additional factors affecting HA composition and filtration in the synovial joint. Specifically, processes such as HA metabolism and mechanical stretching or compression of the synovium may alter the total concentration of HA present in the joint space and the effective membrane pore size, which could be represented as time-dependent variables. It may also be interesting to include other SF molecules, such as albumin or PRG4, in the model. Their large concentration in SF and potential interaction with HA, respectively, may alter HA polarization during filtration. The addition of these factors to the current model would further contribute to an understanding of HA concentration polarization and retention and its effects on permeability in the in vivo synovial joint.

Additional perfusion studies may be conducted in vitro to reflect simulations of normal and diseased synovial joint transport. These studies may be carried out first with HA solutions of varying MW, solute mass, and solution volume, and then with SF,

through semi-permeable membranes and tissue of varying pore size. Measurement of HA concentration at different distances from the membrane and at different times, perhaps by real-time fluorescence imaging with tagged HA or by continuous sampling of perfusate, would help to validate the predictions of dynamic HA concentration polarization in Chapter 2. Experimental measurements of concentration distributions, particularly at and near the membrane, and pressure drops across the membrane would also be useful in better estimating physicochemical parameters for specific HA solutions used in experiments. These parameters could then be used in the theoretical model to better predict pressure drops across the membrane under different flow and membrane situations.

APPENDIX A

EXPERIMENTAL PERFUSION STUDIES OF HYALURONAN SOLUTIONS

A.1 Introduction

Secretion of molecules such as hyaluronan (HA) and proteoglycan 4 (PRG4) is important in the function of synovial fluid (SF) as a biological lubricant, and is regulated by a number of cytokines, including TGF-β1 and IL-1β. Selective filtration of these regulatory cytokines within SF may thus contribute to tissue and SF changes in disease. In normal joints, tissues such as synovium (15-45 nm equivalent pore radius) and articular cartilage provide outflow resistance. Flow through osteochondral tissue is normally limited by the compaction of the cartilage solid matrix; however, cartilage erosion in late-stage osteoarthritis (OA) leads to the exposure of the subchondral bone plate, providing an alternate pathway for filtration from the joint. HA has also been shown to buffer the outflow of fluid under increased pressure by exerting osmotic pressure via a concentration polarized layer at the surfaces of the joint capsule (**Figure A.1**) in a molecular weight (MW)-dependent manner.[1-3] Plasma proteins, namely albumin, can also affect flow resistance in the presence of HA.[4] Changes in HA composition that occur in OA, where HA concentration and MW are decreased, are likely to alter the formation of this layer. We hypothesized that the molecular weight of hyaluronic acid (HA) present in SF alters the filtration of low molecular weight

cytokines from the joint cavity. The objectives of this study were to determine (1) the effect of HA molecular weight on hydraulic conductance, (2) the size selectivity of reflection of HA, and (3) the extent of selective filtration of TGF- β1 and IL-1β, for HA solutions of low and high molecular weights.

A.2 Materials and Methods

Perfusion Testing

Solutions of HA (1 mg/ml), bovine serum albumin (15 mg/ml, MW ~70 kDa), TGF- β1 (13.2 ng/ml, MW 44 kDa), and IL-1β (13.2 ng/ml, MW 30 kDa) in phosphate-buffered saline (PBS) with proteinase inhibitors (PIs) were filtered across a semi-permeable membrane (Whatman, 100 nm pore size) at a constant rate (1.5-5 ul/mn). HA was either of low molecular weight (600-800 kDa) or high molecular weight (Healon, ~4 MDa). The steady-state pressure drop across the sample was measured using a low-range pressure transducer (ΔP = 0-345 kPa). Darcy's law was used to estimate the hydraulic conductance, c, of the combined membrane and concentration polarization layer.

Measurement of Reflection

Membranes and porous frits were sonicated for 10 minutes in PBS+PIs to collect any embedded HA and cytokines. Samples upstream, downstream, and from the membrane and frit were assayed for upstream and downstream cytokine composition by ELISA, albumin composition using the Pierce BCA assay, and HA concentration by ELISA. Size selectivity of HA reflection was assessed by agarose gel electrophoresis followed by band intensity analysis.

Statistics

Data are expressed as mean ± SD, where n=# of samples. Effects of HA molecular weight on hydraulic conductance and individual cytokine reflected fractions were assessed by ANOVA with Tukey post-hoc tests.

A.3 Results

Hydraulic Conductance

Hydraulic conductance was decreased with solutions of HA, albumin, and cytokines TGF- β1 and IL-1β ($p<0.05$, **Figure A.2**). Higher molecular weight HA produced a 2.6-fold larger decrease than lower molecular weight HA in conductance ($P=0.45$), when compared with solutions of albumin alone.

Reflected Fractions

The reflection of HA was correlated with its molecular weight. Agarose gel electrophoresis of the initial, upstream, and downstream solutions for HA of low and high molecular weight showed a polydispersity of the low MW HA between approximately 150-600 kDa, and a MW of the Healon solution of approximately 4 MDa **(Figure A.3)**. The retained fraction of HA upstream was 1.5-fold greater for high MW HA samples **(Figure A.4)**. The reflection coefficient *R* increased from 46.6 to 70.2 when the molecular weight of HA in the perfusate solution was increased.

The reflection coefficient for BSA was 1.9-fold larger for the low MW HA perfusate solutions **(Figure A.5)**. The protein assay was run after only one high MW HA solution had been tested, thus, there is only one data point for the high MW HA group.

Reflected percentages of TGF-β1 were approximately equal for both types of HA solutions **(Figure A.6)**, at 52.3 for the low MW and 50.7 for the high MW. The

reflection coefficient for IL-1β was 2-fold larger for the high MW HA solution than the low MW solution **(Figure A.7)**. The reflection coefficient increased from 42.8 to 87.3 with the substitution of high MW HA for low MW HA. The two other data points for the high MW HA group were omitted due to differences in the mass and aliquot of IL-1β added to the perfusate solution. This left only one data point for the high MW HA group.

A.4 Discussion

These results demonstrate the effects of hyaluronan on hydraulic conductance in the synovial joint. The concentration polarization of HA decreases hydraulic conductance, potentially altering the efflux of important regulatory cytokines from the synovial joint. Compromising of this mechanism due to cleavage of HA, such as in OA, could lead to increased fluid depressurization and selective nutrient loss, causing further cartilage damage and progression of the disease.

These preliminary studies give an idea of the effects of HA molecular weight on the filtration of molecules of various sizes through structures with pore sizes on the order of 100 nm, such as calcified cartilage. The use of a low MW HA of greater MW purity (i.e. less polydispersity) could reduce variability, and allow differences in conductance for low and high MW HA solutions to reach statistically significant levels. Digestion of samples with Proteinase K prior to gel electrophoresis would eliminate the large pink bands seen in the downstream sample lanes, and allow for a more accurate assessment of the migration of the HA bands. More accurate estimation of HA concentration in each sample prior to electrophoresis would allow for more accurate dilutions, and subsequent comparison of band intensity across lanes.

The results show a strong trend of greater HA retention upstream with increasing MW. Although the upstream lane for the high MW solution seems to be polydisperse, it is likely that the sonication of the membrane and frit cleaved the HA present in those samples, creating HA of lower MW. Variability between samples within groups may be reduced with better mixing of diluted samples, and the use of purer HA in samples.

Total mass of HA present in solution may also be an important factor in the formation of a concentration polarized layer under increased pressure, and further exploration in this area could prove to be useful in this study.

The protein assay used samples from earlier perfusion tests, when different volumes of perfusate solution were used in different tests. The high MW sample assayed contained an almost 3-fold smaller volume of perfusate than those used in later tests. Because the formation of the HA filtercake may depend on not only MW but also mass of HA present, it is possible that this smaller volume did not allow proper formation of the concentration polarized layer. This would lead to greater filtration of albumin through the membrane, and the lower reflection coefficient observed.

Absorbance values for TGF-β1 samples were below the lowest detectable concentration for the assay, and the standard curve had to be extrapolated to estimate the concentrations present in each sample. The same occurred for the low MW group for the IL-1β assay. Improper activation of the TGF-β1 samples may have led to lower absorbance values. ELISA results for IL-1β suggest increased retention upstream with increased HA MW, although there is only one data point for the high MW group. It is possible that the cytokines used, from prior aliquots, had degraded in solution, leading to lower measured absorbances. Retesting with fresh cytokine solutions may provide more accurate ELISA results.

Overall, the results show that, with further refinement of methods and use of sample molecules of greater purity, decreased molecular weight of HA may be shown to

increase fluid and nutrient loss through a semi-permeable structure of relatively large pore size.

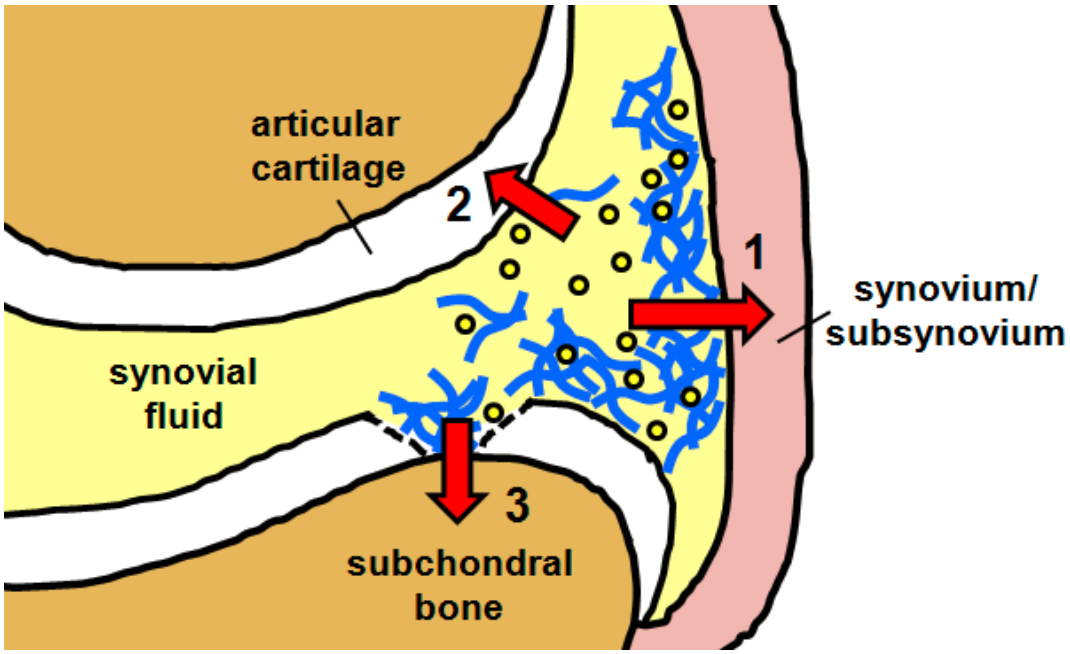

Figure A.1. Schematic of formation of a concentration polarized layer of HA under increased intraarticular pressure through (1) the synovium, (2) articular cartilage, and (3) the subchondral bone plate.

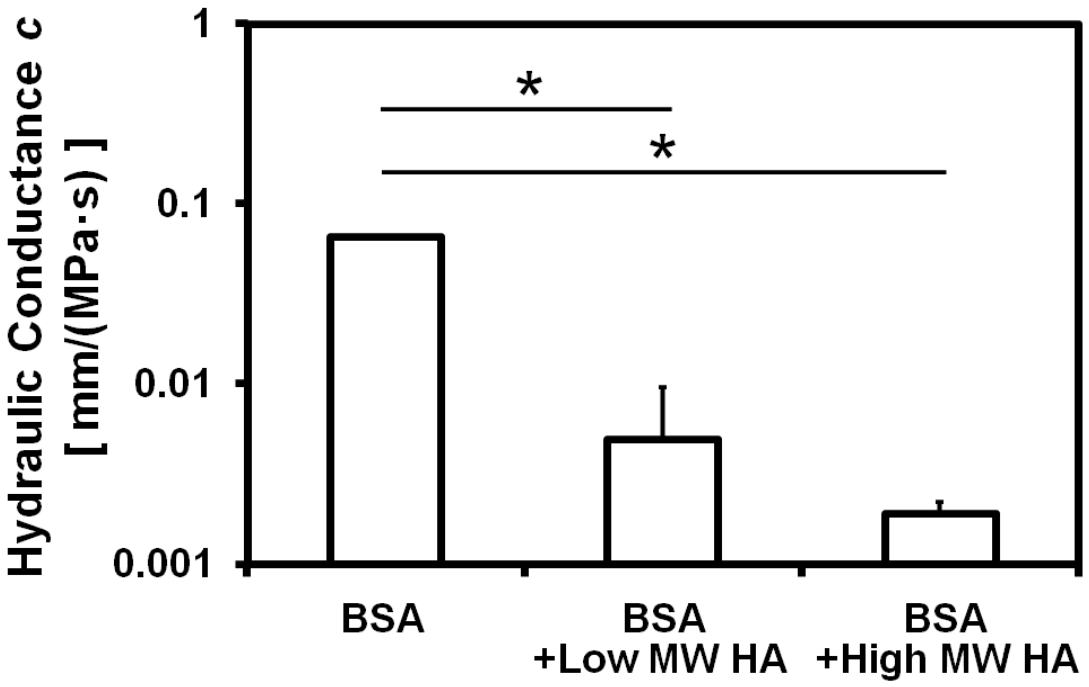

Figure A.2. Effects of molecular weight of HA on hydraulic conductance, (n=3, except n=1 for BSA only). Conductance data are displayed on a log-10 scale.

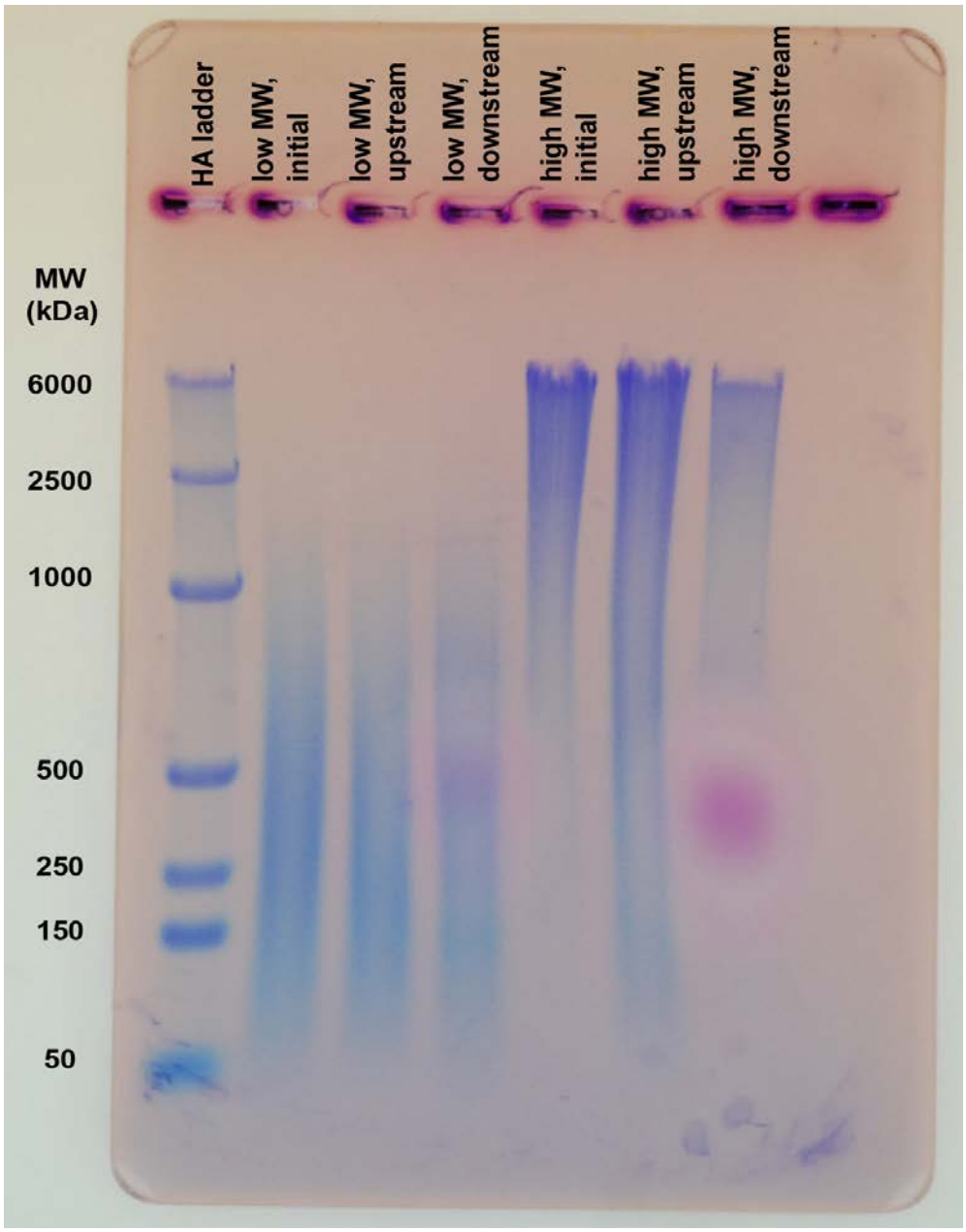

Figure A.3. Molecular weight distribution of HA molecules upstream and downstream after perfusion of low and high molecular weight solutions.

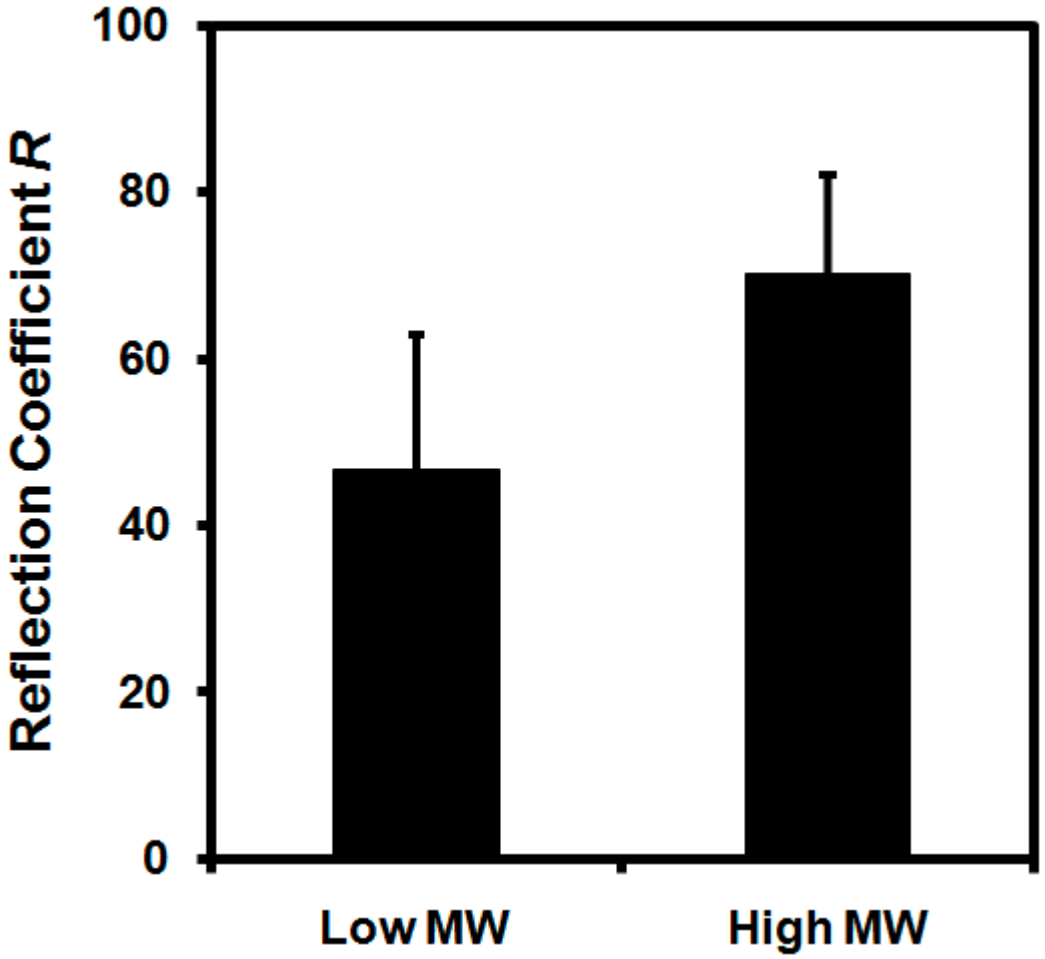

Figure A.4. Effect of HA molecular weight on reflected percentage of HA upstream, n=3.

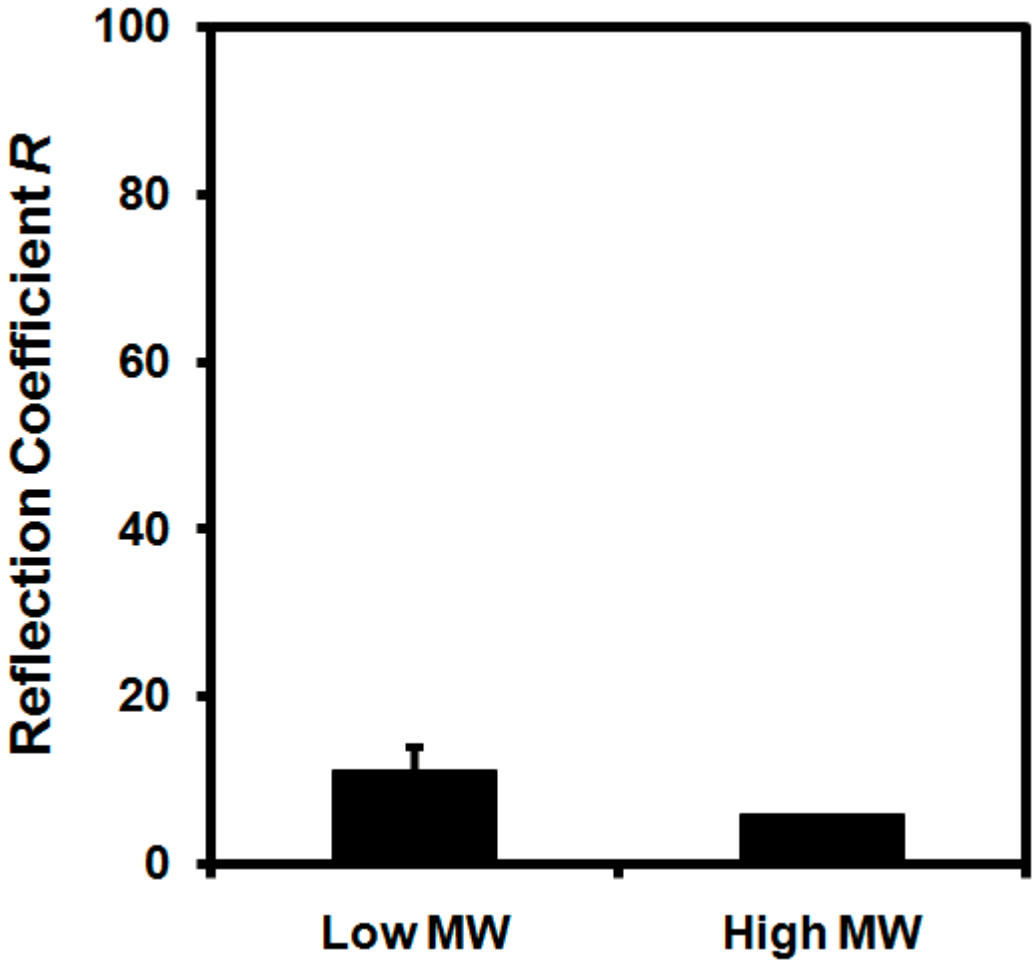

Figure A.5. Effect of HA molecular weight on reflected percentage of BSA upstream (n=3 for low MW, n=1 for high MW).

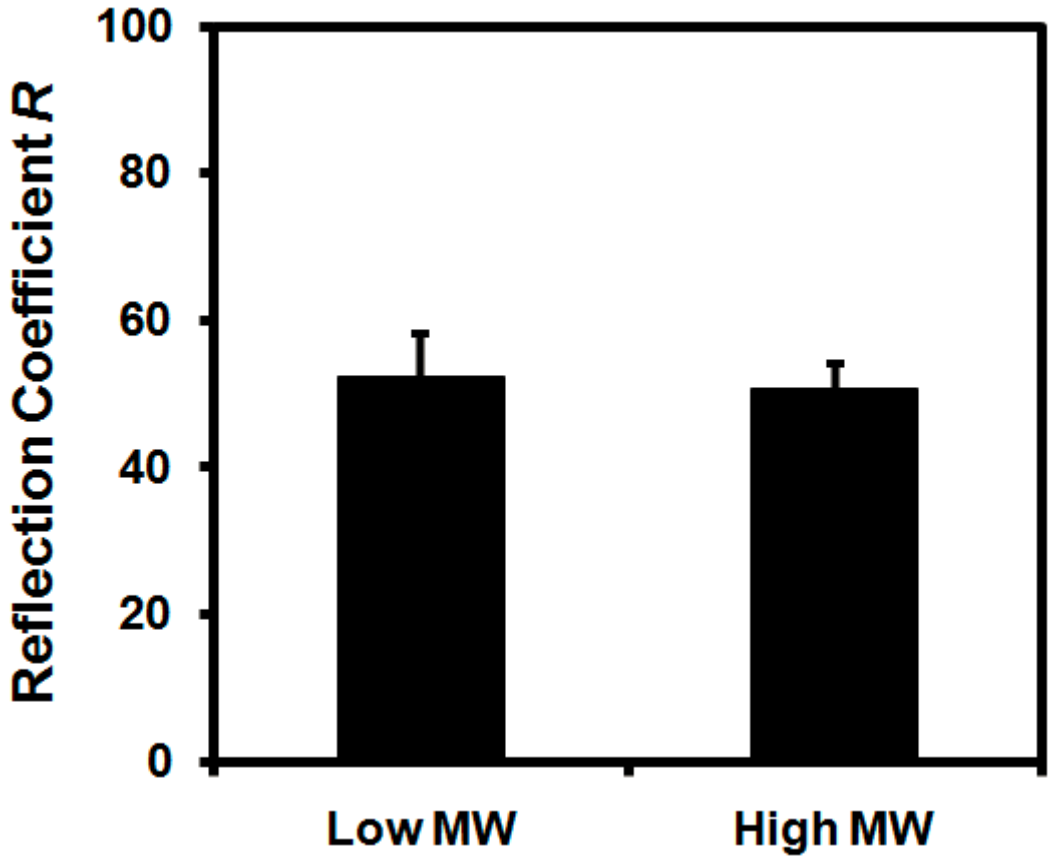

Figure A.6. Effect of HA molecular weight on reflected percentage of TGF-β1 upstream, n=3.

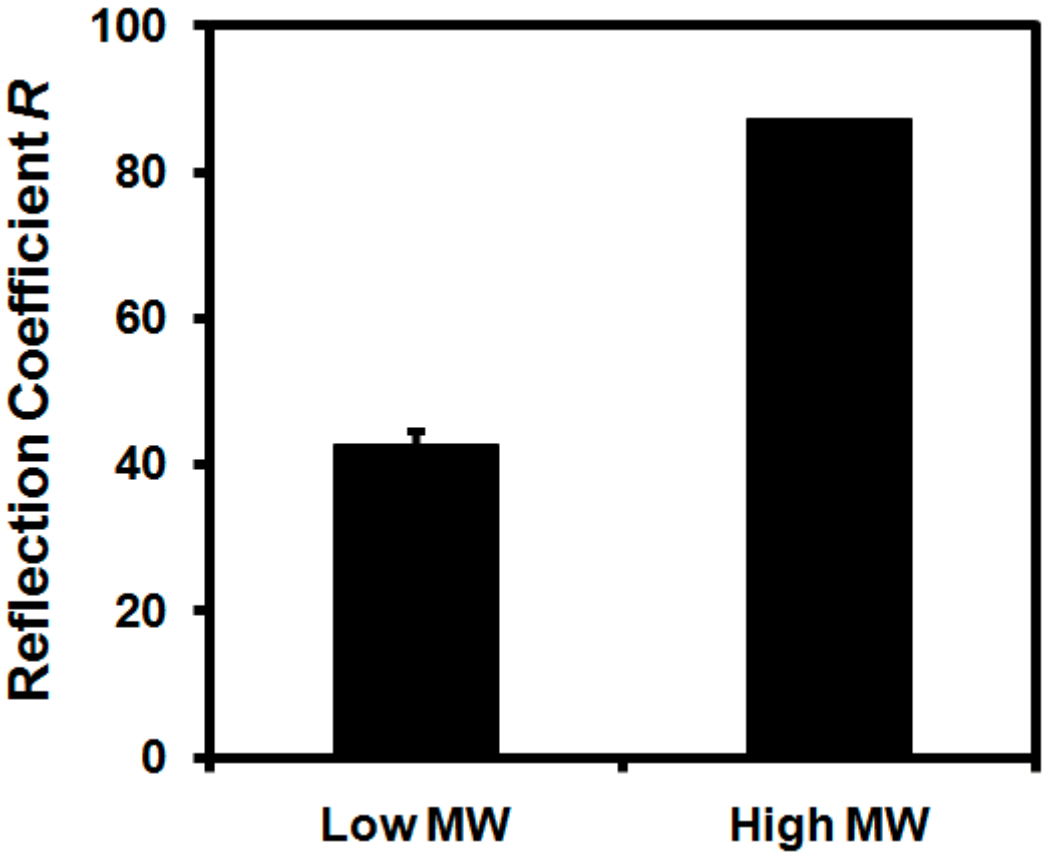

Figure A.7. Effect of HA molecular weight on reflected percentage of IL-1β (n=3 for low MW, n=1 for high MW).

APPENDIX B

MATLAB CODE FOR HA MODEL

B.1 Introduction

The diffusion-convection equation presented in Chapter 2 was solved numerically using MATLAB R2010b to obtain time- and location-dependent predictions for HA concentration.

B.2 Code: Simulation I, Gowman & Ethier

```
function pdexfunc_cte_v3

m = 0;   % declare symmetry of the pde (m is 0 for 1-D slab)

% declare x and t vectors
x = linspace(0,10,9000);   % G&E, BC @ “infinity”
t = linspace(0,180000,900);  % 200 s/step, 50 hrs; G&E

soln = pdepe(m, @pdex_cte, @pdexic_cte, @pdexbc_cte, x, t);
% outputs 3-dimensional array such that:
% sol(:,:,k) approximates component k of the solution u
% sol(i,:,k) approximates component k of solution at time tspan(i) and
mesh points xmesh(:)
% sol(i,j,k) approximates k at tspan(i) and the mesh point xmesh(j)

figure; % 2-D plot at distance of 0 cm
title('Distance of 0cm');
    plot(t/3600,1000*soln(:,1,1))    % convert time axis from s to h
    xlabel('Time  [ hr ]');
    ylabel('Concentration  [ mg / ml ]');
1000*soln(900,1,1)    % print C_mem at end of simulation

figure;
plot(x,1000*soln(1,:,1), x,1000*soln(19,:,1), x,1000*soln(37,:,1),
x,1000*soln(91,:,1), x,1000*soln(181,:,1), x,1000*soln(451,:,1),
x,1000*soln(900,:,1));
xlabel('Distance from Membrane  [ cm ]');
```

```
ylabel('Concentration  [ mg / ml ]');
title('Concentration over Distance at Different Times');
legend('0h','1h','2h','5h','10h','25h','50h')    % G&E

[uout0,duoutdx0] = pdeval(m,x,soln(1,:,1),x);
[uout1,duoutdx1] = pdeval(m,x,soln(19,:,1),x);
[uout2,duoutdx2] = pdeval(m,x,soln(37,:,1),x);
[uout5,duoutdx5] = pdeval(m,x,soln(91,:,1),x);
[uout10,duoutdx10] = pdeval(m,x,soln(181,:,1),x);
[uout25,duoutdx25] = pdeval(m,x,soln(451,:,1),x);
[uout50,duoutdx50] = pdeval(m,x,soln(900,:,1),x);

U = -1.31*(10^-5);       % cm/s, Gowman & Ethier data
D = 2*10^-6;            % cm^2/s

dflux0 = -D*1000*duoutdx0;
dflux1 = -D*1000*duoutdx1;
dflux2 = -D*1000*duoutdx2;
dflux5 = -D*1000*duoutdx5;
dflux10 = -D*1000*duoutdx10;
dflux25 = -D*1000*duoutdx25;
dflux50 = -D*1000*duoutdx50;

cflux0 = U*1000*soln(1,:,1);
cflux1 = U*1000*soln(19,:,1);
cflux2 = U*1000*soln(37,:,1);
cflux5 = U*1000*soln(91,:,1);
cflux10 = U*1000*soln(181,:,1);
cflux25 = U*1000*soln(451,:,1);
cflux50 = U*1000*soln(900,:,1);

% plot of concentration gradient dc/dz
figure;
plot(x,1000*duoutdx0, x,1000*duoutdx1, x,1000*duoutdx2,
x,1000*duoutdx5, x,1000*duoutdx10, x,1000*duoutdx25, x,1000*duoutdx50);
xlabel('Distance from Membrane  [ cm ]');
ylabel('dc/dz  [ mg / cm^4 ]');
axis([0 2 -150 50]);
legend('0h','1h','2h','5h','10h','25h','50h')    % G&E, Barry

% plot of diffusive flux
figure;
plot(x,dflux0, x,dflux1, x,dflux2, x,dflux5, x,dflux10, x,dflux25,
x,dflux50);
xlabel('Distance from Membrane  [ cm ]');
ylabel('Diffusive Flux, -D*dc/dz  [ mg / (s*cm^2) ]');
axis([0 2 -0.0001 0.0003]);
legend('0h','1h','2h','5h','10h','25h','50h')    % G&E, Barry

% plot of convective flux
figure;
plot(x,cflux0, x,cflux1, x,cflux2, x,cflux5, x,cflux10, x,cflux25,
x,cflux50);
xlabel('Distance from Membrane  [ cm ]');
ylabel('Convective Flux, U*c(z,t)  [ mg / (s*cm^2) ]');
axis([0 2 -0.0003 0.0001]);
legend('0h','1h','2h','5h','10h','25h','50h')    % G&E, Barry
```

```
% plot of net flux
figure;
plot(x,(dflux0+cflux0), x,(dflux1+cflux1), x,(dflux2+cflux2),
x,(dflux5+cflux5), x,(dflux10+cflux10), x,(dflux25+cflux25),
x,(dflux50+cflux50));
xlabel('Distance from Membrane  [ cm ]');
ylabel('Net Flux  [ mg / (s*cm^2) ]');
axis([0 2 -0.0001 0.00005]);
legend('0h','1h','2h','5h','10h','25h','50h')    % G&E, Barry

% plot of ratio of diffusive to convective flux
figure;
plot(x,-dflux0./cflux0, x,-dflux1./cflux1, x,-dflux2./cflux2, x,-
dflux5./cflux5, x,-dflux10./cflux10, x,-dflux25./cflux25, x,-
dflux50./cflux50);
xlabel('Distance from Membrane  [ cm ]');
ylabel('Ratio of Diffusive to Convective Flux Magnitude');
axis([0 2 0 10]);
legend('0h','1h','2h','5h','10h','25h','50h')    % G&E, Barry

MW = 434000;     % HA MW, in g/mol
b = 3.34;
dPmem = zeros(900);
for i = 1:900
    dPmem(i) = (8.314472*293*(10^6)*(soln(i,1,1))/MW) +
b*(10^7)*((soln(i,1,1))^2);
end
figure;
plot(t/3600,dPmem/1000);
ylabel('dP_osm  [ kPa ]');
xlabel('Time  [ h ]');
dPmem(900)

% plot total mass HA upstream as a function of time
total_mass = zeros(900);    % vector of masses at each time t
for i = 1:900   % for each time step, solve for total mass upstream
    for j = 1:9000  % numerically estimate area under curve
        total_mass(i) = total_mass(i) +
(soln(i,j,1)*1.27*(10/8999));   % G&E
    end
end
total_mass(900)
figure;
plot(t/3600,1000*total_mass);
xlabel('Time  [ h ]');
ylabel('Total Mass HA Upstream  [ mg ]');

reflection_coeff = zeros(900);
reflection_coeff = (47.341.*soln(:,1,1))+0.287954;  % G&E (434kDa,
15nm)
for i = 1:900
    if reflection_coeff(i) > 1
        reflection_coeff(i) = 1;
    end
end
figure;
plot(t/3600,reflection_coeff);
xlabel('Time  [ h ]');
```

```
ylabel('Reflection Coefficient');

end


function [c,f,s] = pdex_cte(x,t,u,dudx)

U = 1.31*(10^-5);       % Gowman & Ethier data
D = 2*10^-6;

% specifies PDE in time and one space dimension
c = 1;
f = D.*dudx;
s = U.*dudx;      % U*dudx, where U = 6.62E-5 cm/s


function u0 = pdexic_cte(x)

if x < 1.02          % Gowman & Ethier data, l_0 = 1.02 cm
    u0 = 0.004016;  % Gowman & Ethier data, c_0 = 4.016 mg/ml
else
    u0 = 0;
end


function [p1,q1,pr,qr] = pdexbc_cte(x1,u1,xr,ur,t)
% p(x,t,u) + q(x,t)*f(x,t,u,dudx) = 0

if u1 > 0.01504078      % G&E (434 kDa, 15 nm)
    R = 1;
else
    R = (47.341*u1)+0.287954;
end

p1 = u1*1.31*(10^-5)*R;     % Gowman & Ethier data
q1 = 1;                     % D*dC/dx = f
pr = ur;                     % C(infinity,t) = 0
qr = 0;
```

B.3 Code: Simulation II, Perfusion Experiments

```
function pdexfunc_exp

m = 0;   % declare symmetry of the pde (m is 0 for 1-D slab)

% declare x and t vectors (must each contain at least 3 elements)
x = linspace(0,10,9000);   % ultrafiltration, infinity BC
t = linspace(0,18000,900);  % 20 s/step, 5 hrs

soln = pdepe(m, @pdex_exp, @pdexic_exp, @pdexbc_exp, x, t);
% outputs 3-dimensional array such that:
% sol(:,:,k) approximates component k of the solution u
```

```
% sol(i,:,k) approximates component k of solution at time tspan(i) and
mesh points xmesh(:)
% sol(i,j,k) approximates k at tspan(i) and the mesh point xmesh(j)

u = soln(:,:,1);   % extract first solution component

figure; % 2-D plot at distance of 0 cm
title('Distance of 0cm');
    plot(t/3600,1000*soln(:,1,1))    % convert time axis from s to h
    xlabel('Time  [ hr ]');
    ylabel('Concentration  [ mg / ml ]');

figure;
plot(x,1000*soln(1,:,1), x,1000*soln(91,:,1), x,1000*soln(181,:,1),
x,1000*soln(361,:,1), x,1000*soln(541,:,1), x,1000*soln(721,:,1),
x,1000*soln(900,:,1));
xlabel('Distance from Membrane  [ cm ]');
ylabel('Concentration  [ mg / ml ]');
title('Concentration over Distance at Different Times');
legend('0h','0.5h','1h','2h','3h','4h','5h')

[uout0,duoutdx0] = pdeval(m,x,soln(1,:,1),x);
[uout05,duoutdx05] = pdeval(m,x,soln(91,:,1),x);
[uout1,duoutdx1] = pdeval(m,x,soln(181,:,1),x);
[uout2,duoutdx2] = pdeval(m,x,soln(361,:,1),x);
[uout3,duoutdx3] = pdeval(m,x,soln(541,:,1),x);
[uout4,duoutdx4] = pdeval(m,x,soln(721,:,1),x);
[uout5,duoutdx5] = pdeval(m,x,soln(900,:,1),x);

U = -6.62*(10^-5);       % cm/s
D = 2.1*10^-6;            % cm^2/s

dflux0 = -D*1000*duoutdx0;
dflux05 = -D*1000*duoutdx05;
dflux1 = -D*1000*duoutdx1;
dflux2 = -D*1000*duoutdx2;
dflux3 = -D*1000*duoutdx3;
dflux4 = -D*1000*duoutdx4;
dflux5 = -D*1000*duoutdx5;

cflux0 = U*1000*soln(1,:,1);
cflux05 = U*1000*soln(91,:,1);
cflux1 = U*1000*soln(181,:,1);
cflux2 = U*1000*soln(361,:,1);
cflux3 = U*1000*soln(541,:,1);
cflux4 = U*1000*soln(721,:,1);
cflux5 = U*1000*soln(900,:,1);

% plot of concentration gradient dc/dz
figure;
plot(x,1000*duoutdx0, x,1000*duoutdx05, x,1000*duoutdx1,
x,1000*duoutdx2, x,1000*duoutdx3, x,1000*duoutdx4, x,1000*duoutdx5);
xlabel('Distance from Membrane  [ cm ]');
ylabel('dc/dz  [ mg / cm^4 ]');
axis([0 1 -1000 100]);
legend('0h','0.5h','1h','2h','3h','4h','5h')

% plot of diffusive flux
```

```
figure;
plot(x,dflux0, x,dflux05, x,dflux1, x,dflux2, x,dflux3, x,dflux4,
x,dflux5);
xlabel('Distance from Membrane  [ cm ]');
ylabel('Diffusive Flux, -D*dc/dz  [ mg / (s*cm^2) ]');
axis([0 2 -0.0005 0.0025]);
legend('0h','0.5h','1h','2h','3h','4h','5h')

% plot of convective flux
figure;
plot(x,cflux0, x,cflux05, x,cflux1, x,cflux2, x,cflux3, x,cflux4,
x,cflux5);
xlabel('Distance from Membrane  [ cm ]');
ylabel('Convective Flux, U*c(z,t)  [ mg / (s*cm^2) ]');
axis([0 2 -0.0025 0.0005]);
legend('0h','0.5h','1h','2h','3h','4h','5h')

% plot of net flux
figure;
plot(x,(dflux0+cflux0), x,(dflux05+cflux05), x,(dflux1+cflux1),
x,(dflux2+cflux2), x,(dflux3+cflux3), x,(dflux4+cflux4),
x,(dflux5+cflux5));
xlabel('Distance from Membrane  [ cm ]');
ylabel('Net Flux  [ mg / (s*cm^2) ]');
axis([0 2 -0.0002 0.0001]);
legend('0h','0.5h','1h','2h','3h','4h','5h')

% plot of ratio of diffusive to convective flux
figure;
plot(x,-dflux0./cflux0, x,-dflux05./cflux05, x,-dflux1./cflux1, x,-
dflux2./cflux2, x,-dflux3./cflux3, x,-dflux4./cflux4, x,-
dflux5./cflux5);
xlabel('Distance from Membrane  [ cm ]');
ylabel('Ratio of Diffusive to Convective Flux Magnitude');
axis([0 2 -1 5]);
legend('0h','0.5h','1h','2h','3h','4h','5h')

% plot osmotic pressure across membrane surface as a fxn of time
% dPosm = zeros(900);    % vector of pressures at each time t
MW = 4000000;     % HA MW, in g/mol
b = 3.34;

dPmem = zeros(900);
for i = 1:900
    dPmem(i) = (8.314472*293*(10^6)*(soln(i,1,1))/MW) +
b*(10^7)*((soln(i,1,1))^2);
end
dPmem = (dPmem)./1000;  % in kPa
figure;
plot(t/3600,dPmem);
ylabel('Pressure  [ kPa ]');
xlabel('Time  [ h ]');

% plot total mass HA upstream as a function of time
total_mass = zeros(900);    % vector of masses at each time t
for i = 1:900   % for each time step, solve for total mass upstream
    for j = 1:9000  % numerically estimate area under curve
```

```
        total_mass(i) = total_mass(i) +
(soln(i,j,1)*0.50353*(10/8999));   % exp, Lx10
    end
end
total_mass(900)
figure;
plot(t/3600,1000*total_mass);
xlabel('Time  [ h ]');
ylabel('Total Mass HA Upstream  [ mg ]');

reflection_coeff = zeros(900);
reflection_coeff = (47.341.*soln(:,1,1))+0.409624;  % exp
for i = 1:900
    if reflection_coeff(i) > 1
        reflection_coeff(i) = 1;
    end
end
figure;
plot(t/3600,reflection_coeff);
xlabel('Time  [ h ]');
ylabel('Reflection Coefficient');

end


function [c,f,s] = pdex_exp(x,t,u,dudx)

U = 6.62*(10^-5);
D = 2.1*10^-6;

c = 1;
f = D.*dudx;
s = U.*dudx;      % U*dudx, where U = 6.62E-5 cm/s
end


function u0 = pdexic_exp(x)

if x < 0.994
    u0 = 0.0015*heaviside(x);
else
    u0 = 0;
end
end

function [p1,q1,pr,qr] = pdexbc_exp(x1,u1,xr,ur,t)
% p(x,t,u) + q(x,t)*f(x,t,u,dudx) = 0

if u1 > 0.01247071
    R = 1;
else
    R = (47.341*u1)+0.409624;
end

p1 = u1*6.62*(10^-5)*R;
q1 = 1;                      % D*dC/dx = f
pr = ur;                      % C(infinity,t) = 0
```

```
qr = 0;
end
```

B.4 Code: Simulation III, Normal Knee Joint

```
function pdexfunc_normal

m = 0;   % declare symmetry of the pde (m is 0 for 1-D slab)

% declare x and t vectors (must each contain at least 3 elements)
x = linspace(0,0.00361,1000);   % normal physiol
t = linspace(0,90,900);  % 0.1s/step, 1.5 min

soln = pdepe(m, @pdex_normal, @pdexic_normal, @pdexbc_normal, x, t);
% outputs 3-dimensional array such that:
% sol(:,:,k) approximates component k of the solution u
% sol(i,:,k) approximates component k of solution at time tspan(i) and
mesh points xmesh(:)
% sol(i,j,k) approximates k at tspan(i) and the mesh point xmesh(j)

u = soln(:,:,1);   % extract first solution component

figure; % 2-D plot at distance of 0 cm
title('Distance of 0cm');
    plot(t/60,1000*soln(:,1,1))     % convert time axis from s to min
    xlabel('Time  [ min ]');
    ylabel('Concentration  [ mg / ml ]');

figure;
plot(x*10000,1000*soln(1,:,1), x*10000,1000*soln(2,:,1),
x*10000,1000*soln(6,:,1), x*10000,1000*soln(11,:,1),
x*10000,1000*soln(101,:,1), x*10000,1000*soln(601,:,1));
% physiological, 1.5 min total, plot first minute only
xlabel('Distance from Membrane  [ um ]');
ylabel('Concentration  [ mg / ml ]');
title('Concentration over Distance at Different Times');
legend('0s','0.1s','0.5s','1s','10s','60s');

[uout0,duoutdx0] = pdeval(m,x,soln(1,:,1),x);
[uout01,duoutdx01] = pdeval(m,x,soln(2,:,1),x);
[uout05,duoutdx05] = pdeval(m,x,soln(6,:,1),x);
[uout1,duoutdx1] = pdeval(m,x,soln(11,:,1),x);
[uout10,duoutdx10] = pdeval(m,x,soln(101,:,1),x);
[uout60,duoutdx60] = pdeval(m,x,soln(601,:,1),x);

figure;
plot(x*10000,1000*duoutdx0, x*10000,1000*duoutdx01,
x*10000,1000*duoutdx05, x*10000,1000*duoutdx1, x*10000,1000*duoutdx10,
x*10000,1000*duoutdx60);
xlabel('Distance from Membrane  [ um ]');
ylabel('dc/dz  [ mg / cm^4 ]');
axis([0 40 -30 10]);
legend('0s','0.1s','0.5s','1s','10s','60s');

% plot osmotic pressure across membrane surface as a fxn of time
% dPosm = zeros(900);    % vector of pressures at each time t
```

```
% MW = 1900000;     % HA MW, in g/mol
MW = 2700000;
b = 3.34;

dPmem = zeros(900);
for i = 1:900
    dPmem(i) = (8.314472*293*(10^6)*(soln(i,1,1))/MW) +
b*(10^7)*((soln(i,1,1))^2);
end
dPmem = (dPmem)./1000;  % in kPa
figure;
plot(t/60,dPmem);
ylabel('Pressure  [ kPa ]');
xlabel('Time  [ min ] ');

% plot total mass HA upstream as a function of time
total_mass = zeros(900);    % vector of masses at each time t
for i = 1:900   % for each time step, solve for total mass upstream
    for j = 1:1000  % numerically estimate area under curve
        total_mass(i) = total_mass(i) +
(soln(i,j,1)*277*(0.00361/999));   % physiol
    end
end
mass_end = 1000*total_mass(900)
figure;
plot(t/60,1000*total_mass);
xlabel('Time  [ min ]');
ylabel('Total Mass HA Upstream  [ mg ]');

reflection_coeff = zeros(900);
reflection_coeff = (47.341.*soln(:,1,1))+0.238; % physiol; 1.9 MDa, 45
nm
for i = 1:900
    if reflection_coeff(i) > 1
        reflection_coeff(i) = 1;
    end
%     reflection_coeff(i) = 1;
end
figure;
plot(t/60,reflection_coeff);
xlabel('Time  [ min ]');
ylabel('Reflection Coefficient');

end


function [c,f,s] = pdex_normal(x,t,u,dudx)

U = 6.438*(10^-7);     % for 10.7 ul/mn (Levick & McDonald 1995)

D = 1*10^-6;

% specifies PDE in time and one space dimension
c = 1;
f = D.*dudx;
s = U.*dudx;      % U*dudx, where U = 6.62E-5 cm/s
end
```

```
function u0 = pdexic_normal(x)

if x < 0.00361      % physiol
    u0 = 0.004;
else
    u0 = 0;
end
end


function [p1,q1,pr,qr] = pdexbc_normal(x1,u1,xr,ur,t)
% p(x,t,u) + q(x,t)*f(x,t,u,dudx) = 0

if u1 > 0.016096      % normal physiol, low end, 1.9MDa 45 nm
    R = 1;
else
    R = (47.341*u1)+0.238;
end

%R = 1;      % normal physiol, high

p1 = u1*1*6.438*(10^-7)*R;
q1 = 1;                         % D*dC/dx = f
pr = ur*1*6.438*(10^-7);
qr = 1;
end
```

B.5 Code: Simulation IV, Abnormal Knee Joint

```
function pdexfunc_disease

m = 0;   % declare symmetry of the pde (m is 0 for 1-D slab)

% declare x and t vectors (must each contain at least 3 elements)
x = linspace(0,0.1083,1000);    % disease
t = linspace(0,18000,900);  % 20 s/step, 5 hrs
%t = linspace(0,360000,900);     % 100 hrs

soln = pdepe(m, @pdex_disease, @pdexic_disease, @pdexbc_disease, x,
t);
% outputs 3-dimensional array such that:
% sol(:,:,k) approximates component k of the solution u
% sol(i,:,k) approximates component k of solution at time tspan(i) and
mesh points xmesh(:)
% sol(i,j,k) approximates k at tspan(i) and the mesh point xmesh(j)

u = soln(:,:,1);   % extract first solution component

figure; % 2-D plot at distance of 0 cm
title('Distance of 0cm');
```

```
    plot(t/3600,1000*soln(:,1,1))    % convert time axis from s to h
    xlabel('Time  [ hr ]');
    ylabel('Concentration  [ mg / ml ]');

figure;
plot(x,1000*soln(1,:,1), x,1000*soln(91,:,1), x,1000*soln(181,:,1),
x,1000*soln(361,:,1), x,1000*soln(541,:,1), x,1000*soln(721,:,1),
x,1000*soln(900,:,1));
% for 5 hr
%plot(x,1000*soln(1,:,1), x,1000*soln(46,:,1), x,1000*soln(91,:,1),
x,1000*soln(181,:,1), x,1000*soln(451,:,1), x,1000*soln(900,:,1));
%disease, for 100 hrs
xlabel('Distance from Membrane  [ cm ]');
ylabel('Concentration  [ mg / ml ]');
title('Concentration over Distance at Different Times');
legend('0h','0.5h','1h','2h','3h','4h','5h')
%legend('0h','5h','10h','20h','50h','100h')    % G&E, Barry, disease

[uout0,duoutdx0] = pdeval(m,x,soln(1,:,1),x);
[uout5,duoutdx5] = pdeval(m,x,soln(46,:,1),x);
[uout10,duoutdx10] = pdeval(m,x,soln(91,:,1),x);
[uout20,duoutdx20] = pdeval(m,x,soln(181,:,1),x);
[uout50,duoutdx50] = pdeval(m,x,soln(451,:,1),x);
[uout100,duoutdx100] = pdeval(m,x,soln(900,:,1),x);

figure;
plot(x,1000*duoutdx0, x,1000*duoutdx5, x,1000*duoutdx10,
x,1000*duoutdx20, x,1000*duoutdx50, x,1000*duoutdx100);
xlabel('Distance from Membrane  [ cm ]');
ylabel('dc/dz  [ mg / cm^4 ]');
axis([0 0.12 -6 2]);
legend('0h','5h','10h','20h','50h','100h')

% plot osmotic pressure across membrane surface as a fxn of time
% dPosm = zeros(900);    % vector of pressures at each time t
%MW = 700000;  % 0.7 MDa, high end (Dahl)
MW = 300000;   % 300 kDa, low end (Dahl)
b = 3.34;

dPmem = zeros(900);
for i = 1:900
    dPmem(i) = (8.314472*293*(10^6)*(soln(i,1,1))/MW) +
b*(10^7)*((soln(i,1,1))^2);
end
dPmem = (dPmem)./1000;  % in kPa
figure;
plot(t/3600,dPmem);
xlabel('Time  [ hr ]');
ylabel(' Pressure  [ kPa ]');

% plot total mass HA upstream as a function of time
total_mass = zeros(900);    % vector of masses at each time t
for i = 1:900   % for each time step, solve for total mass upstream
    for j = 1:1000  % numerically estimate area under curve
        total_mass(i) = total_mass(i) +
(soln(i,j,1)*277*(0.1083/999)); % disease
    end
end
```

```
total_mass(900)
figure;
plot(t/3600,1000*total_mass);
xlabel('Time  [ hr ]');
ylabel('Total Mass HA Upstream  [ mg ]');

reflection_coeff = zeros(900);
%reflection_coeff = (47.341.*soln(:,1,1))+0.003088;   % disease; 0.3
MDa, 150 nm
reflection_coeff = (47.341.*soln(:,1,1))+0.068322;  % disease; 0.7
MDa, 50 nm
for i = 1:900
    if reflection_coeff(i) > 1
        reflection_coeff(i) = 1;
    end
end
figure;
plot(t/3600,reflection_coeff);
xlabel('Time  [ hr ]');
ylabel('Reflection Coefficient');

end


function [c,f,s] = pdex_disease(x,t,u,dudx)

U = 6.438*(10^-7);     % for 10.7 ul/mn (Levick & McDonald 1995)

D = 0.1*10^-6;

% specifies PDE in time and one space dimension
c = 1;
f = D.*dudx;
s = U.*dudx;      % U*dudx, where U = 6.62E-5 cm/s
end


function u0 = pdexic_disease(x)

if x < 0.1083   % disease, 30 ml SF
    u0 = 0.001;
else
    u0 = 0;
end
end


function [p1,q1,pr,qr] = pdexbc_disease(x1,u1,xr,ur,t)
% p(x,t,u) + q(x,t)*f(x,t,u,dudx) = 0

% if u1 > 0.0210581      % disease; 300 kDa, 150 nm
%     R = 1;
% else
%     R = (47.341*u1)+0.003088;
% end
```

```
if u1 > 0.01968      % disease; 700 kDa, 50 nm
    R = 1;
else
    R = (47.341*u1)+0.068322;
end

p1 = u1*6.438*(10^-7)*R;
q1 = 1;                      % D*dC/dx = f
pr = ur*6.438*(10^-7);
qr = 1;
end
```

References

1. Alvarogracia JM, Zvaifler NJ, Brown CB, Kaushansky K, Firestein GS: Cytokines in Chronic Inflammatory Arthritis .6. Analysis of the Synovial-Cells Involved in Granulocyte-Macrophage Colony-Stimulating Factor Production and Gene-Expression in Rheumatoid-Arthritis and Its Regulation by Il-1 and Tumor-Necrosis-Factor-Alpha. *Journal of Immunology* 146:3365-71, 1991.

2. Anderson JL, Malone DM: Mechanism of Osmotic Flow in Porous Membranes. *Biophysical Journal* 14:957-82, 1974.

3. Ashhurst DE, Bland YS, Levick JR: An Immunohistochemical Study of the Collagens of Rabbit Synovial Interstitium. *Journal of Rheumatology* 18:1669-72, 1991.

4. Balazs EA: The physical properties of synovial fluid and the special role of hyaluronic acid. In: *Disorders of the knee*, ed. by S Helfet, Lippincott Co., Philadelphia, 1974, 63-75.

5. Balazs EA, Watson D, Duff IF, Roseman S: Hyaluronic Acid in Synovial Fluid .I. Molecular Parameters of Hyaluronic Acid in Normal and Arthritic Human Fluids. *Arthritis and Rheumatism* 10:357-&, 1967.

6. Barry SI, Gowman LM, Ethier CR: Obtaining the concentration-dependent diffusion coefficient from ultrafiltration experiments: Application to hyaluronate. *Biopolymers* 39:1-11, 1996.

7. Bear J. Dynamics of Fluids in Porous Media. New York: Dover Publications; 1972.

8. Blewis ME, Nugent-Derfus GE, Schmidt TA, Schumacher BL, Sah RL: A model of synovial fluid lubricant composition in normal and injured joints. *European Cells & Materials* 13:39-, 2007.

9. Coleman P, Kavanagh E, Mason RM, Levick JR, Ashhurst DE: The proteoglycans and glycosaminoglycan chains of rabbit synovium. *Histochemical Journal* 30:519-24, 1998.

10. Coleman PJ, Scott D, Mason RM, Levick JR: Characterization of the effect of high molecular weight hyaluronan on trans-synovial flow in rabbit knees. *J Physiology* 514:265-82, 1999.

11. Coleman PJ, Scott D, Mason RM, Levick JR: Role of hyaluronan chain length in buffering interstitial flow across synovium in rabbits. *J Physiology* 562:425-34, 2000.

12. Coleman PJ, Scott D, Ray J, Mason RM, Levick JR: Hyaluronan secretion into the synovial cavity of rabbit knees and comparison with albumin turnover. *Journal of Physiology-London* 503:645-56, 1997.

13. Curry FE: Mechanics and thermodynamics of transcapillary exchange. In: *Handbook of Physiology*, ed. by E Renkin, Michel C, American Physiological Society, Bethesda, 1984, 309-74.

14. Dahl LB, Dahl IM, Engstrom-Laurent A, Granath K: Concentration and molecular weight of sodium hyaluronate in synovial fluid from patients with rheumatoid arthritis and other arthropathies. *Ann Rheumatic Dis* 44:817-22, 1985.

15. Davies DV: Synovial Membrane and Synovial Fluid of Joints. *Lancet* 251:815-9, 1946.

16. Eckstein F, Winzheimer M, Hohe J, Englmeier KH, Reiser M: Interindividual variability and correlation among morphological parameters of knee joint cartilage plates: analysis with three-dimensional MR imaging. *Osteoarthritis and Cartilage* 9:101-11, 2001.

17. Ethier CR. Hydrodynamics of flow through gels with applications to the eye, SM Thesis: MIT; 1983.

18. Flory P. Principles of Polymer Chemistry. Ithaca, New York: Cornell University Press; 1971.

19. Fossiez F, Djossou O, Chomarat P, FloresRomo L, AitYahia S, Maat C, Pin JJ, Garrone P, Garcia E, Saeland S, Blanchard D, Gaillard C, DasMahapatra B, Rouvier E, Golstein P, Banchereau J, Lebecque S: T cell interleukin-17 induces stromal cells to produce proinflammatory and hematopoietic cytokines. *Journal of Experimental Medicine* 183:2593-603, 1996.

20. Fraser J, Laurent TC: Hyaluronan. In: *Extracellular Matrix,* ed. by WD Comper, Harwood Academic Publishers, Amsterdam, 1996, 141-99.

21. Gowman LM, Ethier CR: Concentration and concentration gradient measurements in an ultrafiltration concentration polarization layer .2. Application to hyaluronan. *Journal of Membrane Science* 131:107-23, 1997.

22. Haubeck HD, Kock R, Fischer DC, Vandeleur E, Hoffmeister K, Greiling H: Transforming Growth-Factor-Beta-1, a Major Stimulator of Hyaluronan Synthesis in Human Synovial Lining Cells. *Arthritis and Rheumatism* 38:669-77, 1995.

23. Hwang J, Bae WC, Shieu W, Lewis CW, Bugbee WD, Sah RL: Increased hydraulic conductance of human articular cartilage and subchondral bone plate with progression of osteoarthritis. *Arthritis and Rheumatism* 58:3831-42, 2008.

24. Ishiguro N, Ito T, Oguchi T, Kojima T, Iwata H, Ionescu M, Poole AR: Relationships of matrix metalloproteinases and their inhibitors to cartilage proteoglycan and collagen turnover and inflammation as revealed by analyses of synovial fluids from patients with rheumatoid arthritis. *Arthritis and Rheumatism* 44:2503-11, 2001.

25. Jawed S, Gaffney K, Blake DR: Intra-articular pressure profile of the knee joint in a spectrum of inflammatory arthropathies. *Annals of the Rheumatic Diseases* 56:686-9, 1997.

26. Jay GD, Britt DE, Cha CJ: Lubricin is a product of megakaryocyte stimulating factor gene expression by human synovial fibroblasts. *Journal of Rheumatology* 27:594-600, 2000.

27. Johnson M. Transport through the aqueous outflow system of the eye: MIT; 1987.

28. Johnson M, Kamm R, Ethier CR, Pedley T: Scaling laws and the effects of concentration polarization on the permeability of hyaluronic acid. *PhysicoChemical Hydrodynamics* 9:427-41, 1987.

29. Jones GC, Riley GP: ADAMTS proteinases: a multi-domain, multi-functional family with roles in extracellular matrix turnover and arthritis. *Arthritis Research & Therapy* 7:160-9, 2005.

30. Kehlen A, Pachnio A, Thiele K, Langner J: Gene expression induced by interleukin-17 in fibroblast-like synoviocytes of patients with rheumatoid arthritis: upregulation of hyaluronan-binding protein TSG-6. *Arthritis Research & Therapy* 5:R186-R92, 2003.

31. Knight AD, Levick JR: The Influence of Blood-Pressure on Trans-Synovial Flow in the Rabbit. *Journal of Physiology-London* 349:27-42, 1984.

32. Knight AD, Levick JR: Morphometry of the Ultrastructure of the Blood Joint Barrier in the Rabbit Knee. *Quarterly Journal of Experimental Physiology and Cognate Medical Sciences* 69:271-88, 1984.

33. Lee DJ: Filter medium clogging during cake filtration. *AIChE Journal* 43:273-6, 1997.

34. Levick JR: Flow through interstitium and other fibrous matrices. *Quarterly J of Exper Phys* 72:409-38, 1987.

35. Levick JR: Synovial fluid hydraulics. *Sci Med* 3:52-61, 1996.

36. Lu Y, Levick JR, Wang W: Concentration polarization of hyaluronan on the surface of the synovial lining of infused joints. *J Physiology* 561:559-73, 2004.

37. Lu Y, Levick JR, Wang W: The mechanism of synovial fluid retention in pressurized joint cavities. *Microcirculation* 12:581-95, 2005.

38. Mansour JM, Mow VC: Permeability of Articular-Cartilage under Compressive Strain and at High-Pressures. *Journal of Bone and Joint Surgery-American Volume* 58:509-16, 1976.

39. Maroudas A: Physicochemical Properties of Cartilage in Light of Ion Exchange Theory. *Biophysical Journal* 8:575-&, 1968.

40. Maroudas A: Physicochemical properties of articular cartilage. In: *Adult articular cartilage,* ed. by M Freeman, Pitman Medical Publishers, Tunbridge Wells, UK, 1979, 215-90.

41. Maroudas A, Bullough P: Permeability of Articular Cartilage. *Nature* 219:1260-&, 1968.

42. Mazzucco D, Scott R, Spector M: Composition of joint fluid in patients undergoing total knee replacement and revision arthroplasty: correlation with flow properties. *Biomaterials* 25:4433-45, 2004.

43. McCutchen C: The frictional properties of animal joints. *Wear* 5:1-17, 1962.

44. McDonald JN, Levick JR: Hyaluronan reduces fluid escape rate from rabbit knee joints disparately from its effect on fluidity. *Exper Physiol* 79:103-6, 1994.

45. McDonald JN, Levick JR: Effect of intra-articular hyaluronan on pressure-flow relation across synovium in anaesthesized rabbits. *J Physiology* 485:179-93, 1995.

46. Miossec P, Chabaud M, Garnero P, Dayer JM, Guerne PA, Fossiez F: Contribution of interleukin 17 to synovium matrix destruction in rheumatoid arthritis. *Cytokine* 12:1092-9, 2000.

47. Momberger TS, Levick JR, Mason RM: Hyaluronan secretion by synoviocytes is mechanosensitive. *Matrix Biology* 24:510-9, 2005.

48. Mow VC, Holmes MH, Lai WM: Fluid Transport and Mechanical-Properties of Articular-Cartilage - a Review. *Journal of Biomechanics* 17:377-94, 1984.

49. Munch W, Zestar L, Anderson J: Rejection of polyelectrolytes from microporous membranes. *J Memb Sci* 5:77-102, 1979.

50. Nade S, Newbold PJ: Factors Determining the Level and Changes in Intra-Articular Pressure in the Knee-Joint of the Dog. *Journal of Physiology-London* 338:21-36, 1983.

51. Ogston AG: On Interaction of Solute Molecules with Porous Networks. *Journal of Physical Chemistry* 74:668-&, 1970.

52. Ogston AG, Stanier JE: The Physiological Function of Hyaluronic Acid in Synovial Fluid - Viscous, Elastic and Lubricant Properties. *Journal of Physiology-London* 119:244-52, 1953.

53. Pelletier JP, Jovanovic DV, Di Battista JA, Martel-Pelletier J, Jolicoeur FC, He Y, Zhang M, Mineau F: IL-17 stimulates the production and expression of proinflammatory cytokines, IL-beta and TNF-alpha, by human macrophages. *Journal of Immunology* 160:3513-21, 1998.

54. Peppin SSL, Elliott JAW: Non-equilibrium thermodynamics of concentration polarization. *Advances in Colloid and Interface Science* 92:1-72, 2001.

55. Price FM, Levick JR, Mason RM: Glycosaminoglycan concentration in synovium and other tissues of rabbit knee in relation to synovial hydraulic resistance. *Journal of Physiology-London* 495:803-20, 1996.

56. Price FM, Mason RM, Levick JR: Radial organization of interstitial exchange pathway and influence of collagen in synovium. *Biophys J* 69:11, 1995.

57. Ropes MW, Rossmeisl EC, Bauer W: The origin and nature of normal human synovial fluid. *Journal of Clinical Investigation* 19:795-9, 1940.

58. Sabaratnam S, Arunan V, Coleman PJ, Mason RM, Levick JR: Size selectivity of hyaluronan molecular sieving by extracellular matrix in rabbit synovial joints. *J Physiology* 567:569-81, 2005.

59. Sabaratnam S, Coleman PJ, Mason RM, Levick JR: Interstitial matrix proteins determine hyaluronan reflection and fluid retention in rabbit joints: effect of protease. *J Physiology* 578:291-9, 2007.

60. Sabaratnam S, Mason RM, Levick JR: Molecular sieving of hyaluronan by synovial interstitial matrix and lymphatic capillary endotheliurn evaluated by lymph analysis in rabbits. *Microvascular Research* 66:227-36, 2003.

61. Sabaratnam S, Mason RM, Levick JR: Filtration rate dependence of hyaluronan reflection by joint-to-lymph barrier: evidence for concentration polarisation. *Journal of Physiology-London* 557:909-22, 2004.

62. Scott D, Coleman PJ, Mason RM, Levick JR: Direct evidence for the partial reflection of hyaluronan molecules by the lining of rabbit knee joints during trans-synovial flow. *Journal of Physiology-London* 508:619-23, 1998.

63. Scott D, Levick JR, Miserocchi G: Non-linear dependence of interstitial fluid pressure on joint cavity pressure and implications for interstitial resistance in rabbit knee. *Acta Physiologica Scandinavica* 179:93-101, 2003.

64. Smith MM, Ghosh P: The Synthesis of Hyaluronic-Acid by Human Synovial Fibroblasts Is Influenced by the Nature of the Hyaluronate in the Extracellular Environment. *Rheumatology International* 7:113-22, 1987.

65. Swann DA, Silver FH, Slayter HS, Stafford W, Shore E: The Molecular-Structure and Lubricating Activity of Lubricin Isolated from Bovine and Human Synovial-Fluids. *Biochemical Journal* 225:195-201, 1985.

66. Wijmans JG, Nakao S, Vandenberg JWA, Troelstra FR, Smolders CA: Hydrodynamic Resistance of Concentration Polarization Boundary-Layers in Ultrafiltration. *Journal of Membrane Science* 22:117-35, 1985.

67. Wik KO, Comper WD: Hyaluronate diffusion in semidilute solutions. *Biopolymers* 21:583-99, 1982.